

A review of continuous contact-force models in multibody dynamics

Luka Skrinjar¹, Janko Slavič^{2,*}, Miha Boltežar²

¹MAHLE Electric Drives Slovenija d.o.o., Šempeter pri Gorici, Slovenia.

²Faculty of Mechanical Engineering, University of Ljubljana, Slovenia.

* janko.slavic@fs.uni-lj.si

July 23, 2018

Abstract

Cite as: Luka Skrinjar, Janko Slavič, Miha Boltežar: A review of continuous contact-force models in multibody dynamics, International Journal of Mechanical Sciences Volume 145, September 2018, Pages 171-187. <https://doi.org/10.1016/j.ijmecsci.2018.07.010>

This is a review of well established and recently introduced contact-force models that are used in the dynamical analysis of multibody systems. In particular, two contact groups have been investigated: the general (point contact) and the cylindrical (line contact) models. For the point-contacts group, 20 different models are listed and a dozen are used in numerical simulations for comparison. While for the cylindrical-contacts group 10 models are listed and most of them are compared on the basis of results of numerical simulations.

Basic numerical experiments are used to compare the evolution of the contact force during the contact process for the presented general contact-force models with energy dissipation and cylindrical contact-force models with and without energy dissipation at the contacts. The effects of the different hysteresis-damping models on the presented general contact-force models are compared. Furthermore, the cylindrical contact-force models are compared in terms of the contact force and the hysteresis damping in the contact.

The objective of this review is to offer basic guidelines for the selection of the proper contact formulation for a specific application in the analysis of multibody dynamics with continuous contacts-impact events. Twenty general contact-force models are presented in this research and more than 10 cylindrical continuous contact-force models are presented and compared. Furthermore, a hysteresis-damping effect in cylindrical contact-force models is researched and presented.

Keywords contact models, contact forces, multibody dynamics, revolute clearance joints

1 Introduction

Research activities in the area of multibody dynamics have increased significantly in recent decades, mainly due to the market demand for high quality products by the rapid progress in computer technology and the development of appropriate theories of dynamics that enable the modeling of dynamical systems with contacts in a variety of engineering applications, such as: civil and infrastructure applications [1–3], granular materials [4], designing parts or assemblies of mechanical systems [5–10], railway dynamics [11–14], crash analysis [15–17], bio-mechanics [18–24], robotics [25–27], mechanisms [28–32], vibro-impact drilling [33], bearing elements [34] and others [35,36]. Multibody dynamics can be categorized as the study of mechanical systems assembled from several bodies that are interconnected with kinematic constraints that restrict their relative movement and are subjected to the acting external forces [37,38]. These forces can include inertia or gravitational forces, state-dependent forces or contact forces generated by the contacts between the bodies. The intensive impact can often result in limited operation or the failure of a mechanical system due to vibration [39], load propagation [40], fatigue [41], cracks [42], wear [43] or any other cause, leading to a non-functional state.

It is important to mention that the bodies that are assembled in a multibody system can be considered as rigid or deformable. A body can be considered as rigid when its deformations are small, such that they do not affect the global motion of the body itself [44]. It is assumed that rigid bodies are a representation of actual mechanical systems, although they are not completely rigid in nature. Many mechanical systems are assembled from rigid and deformable bodies or rigid bodies with soft surfaces or bodies that are rigid enough to be considered rigid overall, although they can experience significant local deformations during the

contact-impact process. Consequently, a contact-evaluation procedure must be able to model the dynamics of the contact between compliant surfaces [45].

In a multibody system impact occurs when two bodies collide [46]. The main properties of the contact-impact process are: very short durations, large contact forces, rapid dissipations of the energy and high accelerations and decelerations of the contacting bodies [47]. The continuous contact-impact process is divided into two phases: compression and restitution. At the beginning of the contact process, the start of the compression phase, the contact force increases simultaneously with the contact deformation and reaches its maximum value at the end of the compression phase. The restitution or expansion phase follows the compression phase, where the energy that is stored during the compression phase drives the bodies in contact apart, and it ends when the two bodies are separated. Consequently, some energy, due to internal damping [48], is lost through vibrations, heat, sound and in other forms [49]. It was found that perfectly elastic collisions between two bodies dissipate energy, due to the transformation of the initial kinetic energy into internal vibrations after contact [50]. Thus, the initially developed elastic models needed to be developed to enable the dissipation of energy during the contact-impact process. One of the most widely used concepts to consider energy dissipation is based on the use of coefficient of restitution. This parameter has different definitions and one of the most popular and commonly used is Newton's law of restitution, also known as the kinematic coefficient of restitution. It is defined as the ratio of the post-impact relative velocity to the pre-impact relative velocity of the body going through the contact-impact process. A positive value of the relative contact velocity in the normal direction between two contact points on each body indicates that the bodies are approaching, during the compression phase, and reaches a value of zero at the point of maximum contact deformation, and a negative value of the relative contact velocity in the normal direction indicates that the bodies are moving away from each other during the restitution phase.

When performing a dynamical analysis of a multibody system it is important to find an accurate time value for the transition between the different states, specifically the transition between the non-contact and the contact states. If the time value at the start of the contact is not detected properly, the initial contact force might become abnormally large due to the artificially large initial indentation between the bodies in contact. This numerical problem leads to an artificial increase in the mechanical energy of the system and can also stall the integration process. To overcome this shortcoming, close control of the numerical procedure, which automatically detects and evaluates all the initial contact situations efficiently, is required [51]. In practice, when working with numerical simulations, most of the processor time is used on contact-detection tasks. The contact between two bodies can be due to the free movement of both bodies or due to the clearances in a mechanical joint (i.e., a planar revolute clearance joint can be considered as a special type of internal contact between the two cylinders) [52–54]. Recently, a unified approach to the modeling of mechanical joints with and without clearances was introduced in the frame of multibody dynamics [55] and the effect of a 3D revolute clearance joint on the engineering application of planar mechanisms was investigated and validated based on experimental data [56]. When working on the numerical simulations of multibody systems [57,58] an experimental investigation [59–62] is also important to successfully characterize the parameters of the dynamics [32,63] or to validate the numerical results [64].

In general, the contact-impact event in multibody dynamics can be evaluated based on the continuous method, also known as the smooth approach, at the force-acceleration level [65], or based on the unilateral geometrical constraints, also known as the non-smooth approach, at the impulse-velocity level [66]. There are three main features that define these two methods: (i) the location of the contact points, (ii) the relative penetration or contact deformation between two bodies and (iii) the contact forces [67]. The contact points on both bodies are coincident, while some local deformation at the contact is allowed with the penalty method. The contact deformation represents a key value as it is used to evaluate the contact force according to the appropriate constitutive law [68].

Another approach to modeling the contact-impact event in the dynamic analysis of multibody systems, for the non-smooth approach, is based on impulse-momentum [69] theory. This has been primarily applied to impacts between rigid bodies [47]. The theory of impulse-momentum used in modeling the contact-impact event assumes that the deformation in the contact remains small in comparison to the overall geometry of the colliding bodies and that the time interval of the contact-impact process is sufficiently brief. Therefore, the potential energy of the mechanical system does not change and so there are no changes in the system configuration and all the other external forces can be considered negligible. The changes in velocity occur instantly, as a result of the large impact forces. When implementing this approach in the computer software code only a minimum penetration is allowed to detect the contact in a numerical manner and this not used to evaluate the size of the contact impulse. The energy-dissipation effect is included via the relation between the impulse of the contact force in the compression and restitution phases and the coefficient of restitution [70].

During the dynamical analysis the state variables of a multibody system during a contact-impact event can

be evaluated using either a continuous or a discontinuous approach. The penalty method is the most frequently used continuous approach, where the contact forces and the deformations are modeled with a set of spring-damper elements that represent the surface compliance of the contact bodies [71]. In the non-smooth approach, the unilateral constraints are solved as a linear complementary problem (LCP) [72–76]. When the contact is considered as a contact between two cylinders based on the continuous approach, a suitable contact-force law should be used. In fact it is advisable [77] to use one of the cylindrical contact-force models summarized in this study, however other models can also be used [67, 78–80].

This work focuses on presenting and reviewing different continuous contact-force models for point and line contacts that have been used in a variety of multibody applications. The evolution of both types of contacts, based on geometry, and the developed contact-force models are presented and compared. Besides the definitions, basic multibody systems are also used for the comparison of the models. The main objective of this manuscript is to provide users with a common platform where they can easily find developed continuous contact-force models, for general and cylindrical contact geometry, and compare them so as to select the most suitable continuous contact-force model. The focus is also on energy-dissipation models, which are compared for general contact force models and further discussed for cylindrical contact-force models.

This study is organized as follows. Section 2 presents the developed general contact-force models that are based on a point contact between two spheres and their comparison based on a simple dynamical system. Section 4 presents the developed cylindrical contact-force models and their comparison based on a simple dynamical system with an internal contact between two cylinders. A discussion about the integration of the dissipation in the cylindrical contact-force models is presented in Section 6. The conclusions are drawn in Section 7.

2 Review of the general contact-force models

The foundations of pure elastic contact-force models were laid by Hertz [81], who concluded that, in general, a contact area was elliptical and no energy dissipation was considered during the contact-impact process. This led several researchers to develop more advanced contact-force models that take this energy dissipation into account.

A thorough overview of general contact-force models was made by [65, 67], while some cylindrical contact-force models were researched and compared by Pereira et al. [77, 82]. For a greater computational efficiency of the numerical simulation and to avoid convergence problems, during each integration time step a contact-force model that represents an explicit correlation between the contact deformation and the contact force is advised [77]. This explicit correlation between the contact deformation and the contact force is defined using the Lankarani-Nikravesh contact-force model for a general contact [71, 83] and has been used in several studies of rigid [84] and rigid-flexible [85] multibody systems. Recently, an enhanced cylindrical contact-force model was developed for an easier implementation in computer software codes [86], and it was also used in research of the dynamics of chain drives using a generalized revolute clearance-joint formulation [87]. The cylindrical contact-force models generally represent the contact force as an implicit function of the contact deformation and do not account for the energy dissipation during the contact process. The lack of energy dissipation with cylindrical contact-force models can be overcome by including the hysteresis damping after the contact force has been evaluated, or by using a model that defines an explicit relationship between the contact deformation and the contact force, such as an enhanced cylindrical contact-force model [86]. In his research Hertz concluded that, in general, a contact surface has an elliptical shape [48, 88, 89]. Hertz's contact law relates the contact force to a nonlinear power function of the indentation and can be expressed as:

$$F_n = K\delta^n, \quad (1)$$

where K is the contact-stiffness parameter, δ represents the relative indentation between the contacting bodies and n is the nonlinear power exponent that is determined from the material and the geometrical properties of the local region of the bodies in contact. These contact parameters, but principally the contact stiffness, can be evaluated numerically [90, 91] or experimentally [92].

The value of the contact-stiffness parameter is evaluated differently for each type of contact geometry, and for a simple geometrical shape the analytical expressions are defined as follow. For the contact between two spheres with radii R_i and R_j the contact stiffness is evaluated as [48]:

$$K = \frac{4}{3(h_i + h_j)} \sqrt{\frac{R_i R_j}{R_i + R_j}}, \quad (2)$$

where h_k is defined for the k -th body as:

$$h_k = \frac{1 - \nu_k^2}{E_k} \quad k = i, j, \quad (3)$$

and the parameters E_k and ν_k are the modulus of elasticity and the Poisson's ratio and are dependent on the material properties. For the contact between a sphere and a plane, the contact stiffness is evaluated as [65]:

$$K = \frac{4\sqrt{R}}{3(h_i + h_j)}, \quad (4)$$

where the parameter R is the radius of the sphere. For the contact between two planar surfaces the contact stiffness is evaluated as [93]:

$$K = \frac{a}{0,475(h_i + h_j)}, \quad (5)$$

and a is the half width of the contact.

It should be emphasized that, based on the definition of the curvature, the radius has negative values for concave surfaces and positive values for convex surfaces [77]. The parameter δ is referred to as the relative penetration depth, i.e., the contact deformation, for two bodies and n is the nonlinear exponent that depends on the material properties and the geometry in the local contact area.

Perfectly elastic contact-force models do not account for the energy dissipation in the contact that is present in mechanical systems. Therefore, it is not possible to model the compression and restitution phase of the contact with the contact model developed by Hertz. The model developed by Kelvin and Voigt is a basic model that includes the energy dissipation and is modeled as a linear spring and a linear damper element [48]. These two models are combined in parallel and the contact force is evaluated as:

$$F_n = K\delta + D\dot{\delta}, \quad (6)$$

where the parameter K represents the linear elastic force, the parameter D represents the force-dissipation (energy-dissipation) coefficient during the contact process and $\dot{\delta}$ is the normal component of the relative contact velocity. Due to its simple definition, this model was used in several studies [94–96]. Khulief and Shabana used the Kelvin-Voigt model for the contact between flexible bodies [97], while it was also used in an evaluation for the vertical contact forces on a tire in vehicle dynamics [98].

The linear Kelvin-Voigt model does not represent the non-linearity of the whole contact process and is only suitable for contacts at higher impact velocities [65]. In the research by Dubowsky et al. it is suggested that the dissipation component of the contact force is a nonlinear function of the contact deformation and the normal component of the relative contact velocity. This has several disadvantages. At the start of the contact process, when the contact deformation is equal to zero [51], the dissipation component of the contact force has a non-zero value, which is physically inconsistent. At the beginning of the contact process the elastic and dissipative components of the contact force have to be equal to zero. Furthermore, at the end of the contact process (i.e., at the end of the restitution phase) the contact deformation depth is equal to zero and the normal component of the relative contact velocity is negative, which is usually physically inconsistent, as two bodies cannot attract each other. During the entire contact process the coefficient of dissipation is constant, which results in a constant dissipation in the compression-and-restitution phase, which is physically inconsistent [99,100]. The model suggested by Hunt and Crossley evaluates the contact process more accurately. In their work Hunt and Crossley state that the exponent of the damping coefficient has to be equal to the exponent of a linear spring. The contact force is based on the Hertzian contact model and the non-linear viscous-elastic element, which accounts for the damping and depends on the penetration depth, and has the form [101]:

$$F_n = K\delta^n + \chi\delta^n\dot{\delta}, \quad (7)$$

where the parameter χ is the hysteresis damping factor and is defined as:

$$\chi = \frac{3}{2} \frac{K}{\dot{\delta}_0} (1 - c_r), \quad (8)$$

where $\dot{\delta}_0$ is the initial relative contact velocity in the normal direction and c_r is the coefficient of restitution.

Eq.(7) can be substituted into Eq.(8) and the contact force can be evaluated using the following form:

$$F_n = K\delta^n \left(1 + \frac{3(1 - c_r)}{2} \frac{\dot{\delta}}{\dot{\delta}_0} \right) \quad (9)$$

Due to the problems associated with evaluating the contact properties, such as the contact stiffness and the coefficient of restitution, Guess et al. used the results obtained from a finite-element analysis to evaluate the contact properties [102]. The model of Hunt and Crossley is best for impacts with a high value of the coefficient of restitution, when the impact typically has a lower energy dissipation, as reported in [25, 103]. The model proposed by Herbert and McWhannell uses the coefficient of restitution as the main element to evaluate the dissipation of mechanical energy during the contact process [104]. The authors used the Hunt-Crossley model and defined the hysteresis-damping factor as:

$$\chi = \frac{6}{(2c_r - 1)^2 + 3} \frac{K}{\dot{\delta}_0} (1 - c_r), \quad (10)$$

The expression for the contact force is defined when Eq.(10) is substituted into Eq.(7):

$$F_n = K\delta^n \left(1 + \frac{6(1 - c_r)}{(2c_r - 1)^2 + 3} \frac{\dot{\delta}}{\dot{\delta}_0} \right). \quad (11)$$

The model of Herbert and McWhannell can be considered as an enhanced Hunt-Crossley model. The difference between the hysteresis-damping factors defined with Eqs. (8) and (10) is equal to 1.5% [104]. This contact model was mostly used in the dynamic analysis of gears [105, 106]. The authors Lee and Wang in [107] suggested a new factor for the hysteresis-damping. The main objective was to fulfill the boundary conditions of the hysteresis-damping factor. Furthermore, the value of the dissipative component of the contact force is equal to zero when the contact deformation is equal to zero and when the normal component of the relative contact velocity is equal to zero. The hysteresis-damping factor is defined as:

$$\chi = \frac{3}{4} \frac{K}{\dot{\delta}_0} (1 - c_r). \quad (12)$$

Eq. (12) can be substituted into Eq. (7) and the normal contact force is evaluated as:

$$F_n = K\delta^n \left(1 + \frac{3}{4} \frac{\dot{\delta}}{\dot{\delta}_0} (1 - c_r) \right). \quad (13)$$

The proposed model is relatively simple to use, but it is not often used in multibody dynamics with contact-impact events. One of the most widely used contact-force models is the Lankarani-Nikravesh model [71]. The hysteresis-damping factor is evaluated based on the loss of kinetic energy that is due to the internal damping. Based on the kinetic energy before and after the contact, the loss of kinetic energy is evaluated as a function of the coefficient of restitution c_r and the normal component of the relative contact velocity at the start of the contact-impact event $\dot{\delta}_0$:

$$\delta E = \frac{1}{2} m \dot{\delta}_0^2 (1 - c_r^2), \quad (14)$$

where m_{eff} is the equivalent mass defined as:

$$m_{eff} = \frac{m_i m_j}{m_i + m_j} \quad (15)$$

and m_i, m_j are the masses of the bodies i and j . The loss of kinetic energy is evaluated by integrating the contact force over time. If it is assumed that the characteristic of the contact force in the compression phase is equal to the restitution phase, the energy loss will be evaluated as:

$$\delta E \simeq \frac{2}{3} \frac{\chi}{K} m \dot{\delta}_0^3. \quad (16)$$

The hysteresis-damping factor χ is defined when Eq. (14) is equal to Eq. (16):

$$\chi = \frac{3}{4} \frac{K}{\dot{\delta}_0} (1 - c_r^2). \quad (17)$$

Eq. (17) is substituted into Eq. (7) and the normal contact force is evaluated as:

$$F_n = K\delta^n \left(1 + \frac{3}{4} \frac{\dot{\delta}}{\dot{\delta}_0} (1 - c_r^2) \right). \quad (18)$$

Eq. (18) is only valid when the initial relative contact velocity in the normal direction is less than the velocity of the propagation of waves in the material defined as:

$$\dot{\delta}_0 \leq 10^{-5} \sqrt{\frac{E}{\rho}}, \quad (19)$$

where ρ is the specific density of the material.

The developed model can be used for general contacts in mechanical systems, especially when the ratio of the lost energy is relatively small. Furthermore, Eq. (18) works well for elastic contacts when the coefficient of restitution has a value close to 1. Shivaswamy has shown that for smaller contact velocities the internal damping has a larger influence on the energy dissipation [108]. The Lankarani-Nikravesh model was used in several studies [109–111] and as a starting point for others who developed new contact-force models based on the Lankarani-Nikravesh model for use in planar mechanical systems with revolute clearance joint [112].

The model of Gonthier et al. is best for larger contact surfaces and defines the hysteresis-damping factor as [103]:

$$\chi = \frac{d K}{c_r \dot{\delta}_0}, \quad (20)$$

where d represents the non-dimensional factor, defined as:

$$1 + \frac{d}{c_r (1-d)} = e^{d(1+\frac{1}{c_r})} \quad (21)$$

and can be approximated with:

$$d \approx 1 - c_r^2. \quad (22)$$

The contact model of Gonthier et al. can be written as:

$$F_n = K \delta^n \left[1 + \frac{1 - c_r^2}{c_r} \frac{\dot{\delta}}{\dot{\delta}_0} \right]. \quad (23)$$

The contact-force model, Eq. (23), is mainly related to force, expressed as an explicit non-linear function of the contact volume and the volume contact stiffness. The unit for contact force is Newton per volume. However, a problem can arise during an evaluation of the parameter for volume stiffness. Zhiying and Qishao developed a contact-force model and defined the hysteresis-damping factor as [113]:

$$\chi = \frac{3(1 - c_r^2) e^{2(1-c_r)} K}{4 \dot{\delta}_0} \quad (24)$$

and the contact force is evaluated as:

$$F_n = K \delta^n \left[1 + \frac{3(1 - c_r^2) e^{2(1-c_r)}}{4} \frac{\dot{\delta}}{\dot{\delta}_0} \right]. \quad (25)$$

The proposed model by Zhiying and Qishao is used in an analysis of the contact, with the goal being to define the correlation between the coefficient of restitution, the contact parameters and the energy dissipated during the contact. Another contact-force model was developed by Flores et al. [114], it is based on Hertz's contact theory together with a hysteresis-damping parameter that includes the loss of energy during the contact process. This loss of energy is evaluated as a function of the coefficient of restitution and the initial contact velocity, as defined by Eq. (16). The dissipated energy is evaluated by integrating of the contact force over the depth of the contact penetration. Flores et al. evaluated the dissipated energy during a contact based on the dynamic model of a simple pendulum in contact with a wall, as follows:

$$\delta E = \frac{1}{4} \chi (1 - c_r) \dot{\delta}_0 \dot{\delta}_{max}^{\frac{5}{2}}, \quad (26)$$

where δ_{max} is the maximum depth of the deformation at the contact. From Eq. (14) and Eq. (26) the hysteresis damping factor can be defined as:

$$\chi = \frac{8(1 - c_r) K}{5c_r \dot{\delta}_0}. \quad (27)$$

The contact force is evaluated as:

$$F_n = K\delta^n \left[1 + \frac{8(1-c_r)}{5c_r} \frac{\dot{\delta}}{\dot{\delta}_0} \right] \quad (28)$$

It must be emphasized that this contact-force model was developed for situations occurring between very elastic and very inelastic contacting materials [65]. Therefore, the suggested expression, Eq.(28), is similar to the contact model developed by Gonthier et al., Eq. (23). The contact model developed by Hu and Guo was intended for use in a contact between softer materials that have a smaller coefficient of restitution, and more elastic contacts with higher values of energy dissipation. These types of contact properties can be found in biomechanical components, bushings, etc. The hysteresis-damping factor is defined based on the concentric impact between two spheres and is [115]:

$$\chi = \frac{3(1-c_r)K}{2c_r \dot{\delta}_0} \quad (29)$$

The contact force is defined with the expression:

$$F_n = K\delta^n \left[1 + \frac{3(1-c_r)}{2c_r} \frac{\dot{\delta}}{\dot{\delta}_0} \right] \quad (30)$$

A comparison with existing contact models shows the usability for soft and hard materials in contact [115].

In the past different formulations of the hysteresis-damping factor were proposed, which are typically functions of the contact stiffness, the initial contact velocity and the coefficient of restitution. Table 1 presents an overview of some of the most popular expressions for the hysteresis-damping factor that have been developed independently by different authors.

3 Comparison of the general contact-force models

A simple dynamic model is used to present the comparison of the listed contact-force models, see Fig. (1). The dynamic system is assembled from two spheres with the radius $R_0 = 0.02$ m and the mass $m = 9.2$ kg. Sphere i has an initial velocity v_0^i , while sphere j is stationary. The relative contact stiffness for the contact between two spheres is equal to 5.2×10^9 N/m^{3/2} and the restitution coefficient c_r is in the range from 0 to 1, to better understand and present the amount of dissipated energy due to the coefficient of restitution.

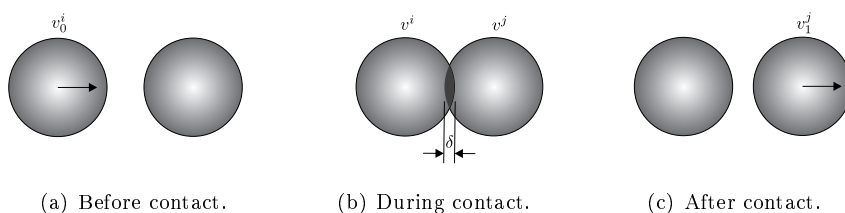


Fig. 1. Contact-impact process between two spheres.

A comparison of the hysteresis-damping factor models that are listed in Table 1 and the use of an analytical function to evaluate the hysteresis-damping factor based on the value of the coefficient of restitution c_r are presented in Fig. 2. It is clear that for values of the coefficient of restitution greater than 0.7 almost all the hysteresis-damping factor values are approximately equal and tend toward zero, when the value of the coefficient of restitution is equal to 1, except for the Gharib-Hurmuzlu model. Therefore, the selection of the contact-force model and its hysteresis-damping factor do not represent major differences for the interval from 0.7 to 1. On the other hand, when the value of the coefficient of restitution is small, i.e., in the interval from 0 to approx. 0.5 large differences in the hysteresis-damping factor are present. Consequently, the selection of the contact-force model and its hysteresis-damping factor can have a great impact on the evaluated value of the contact force.

The evolution of the contact force versus the contact deformation during the contact process for different contact models is presented in Fig. 3. For models that include energy dissipation a greater contact force results in a lower energy loss and a higher relative normal contact velocity at the end of the contact. A comparison of the contact force related to the depth of contact deformation for different values of the coefficient of restitution

Table 1
Contact-force models.

Contact-force model	Constitutive law	n	m	χ
Hertz [81]	$F_n = K\delta^{\frac{3}{2}}$	$\frac{3}{2}$	—	—
Kelvin-Voigt [48]	$F_n = K\delta + \chi\delta\dot{\delta}$	1	1	—
Hunt-Crossley [101] Marefka-Orin [25]	$F_n = K\delta^{\frac{3}{2}} + \chi\delta^{\frac{3}{2}}\dot{\delta}$	$\frac{3}{2}$	$\frac{3}{2}$	$\frac{3(1-c_r)}{2} \frac{K}{\delta_0}$
Herbert-McWhannell [104]	$F_n = K\delta^{\frac{3}{2}} + \chi\delta^{\frac{3}{2}}\dot{\delta}$	$\frac{3}{2}$	$\frac{3}{2}$	$\frac{6(1-c_r)}{(2c_r-1)^2+3} \frac{K}{\delta_0}$
Lee-Wang [107]	$F_n = K\delta^{\frac{3}{2}} + \chi\delta^{\frac{3}{2}}\dot{\delta}$	$\frac{3}{2}$	$\frac{3}{2}$	$\frac{3(1-c_r)}{4} \frac{K}{\delta_0}$
Anagnostopoulos [116]	$F_n = K\delta + \chi\delta\dot{\delta}$	1	1	$2 \frac{-\ln c_r}{\pi^2 + (\ln c_r)^2} \sqrt{K m_{eff}}$
Lankarani-Nikravesh [93]	$F_n = K\delta^{\frac{3}{2}} + \chi\delta^{\frac{3}{2}}\dot{\delta}$	$\frac{3}{2}$	$\frac{3}{2}$	$\frac{3(1-c_r^2)}{4} \frac{K}{\delta_0}$
Ristow [4]	$F_n = K\delta^{\frac{3}{2}} + \chi\delta\dot{\delta}$	$\frac{3}{2}$	1	Empirical value
Tsuji et al. [117]	$F_n = K\delta^{\frac{3}{2}} + \chi\delta^{\frac{1}{4}}\dot{\delta}$	$\frac{3}{2}$	$\frac{1}{4}$	$\alpha\sqrt{K m_{eff}}$
Lee-Herrmann [118]	$F_n = K\delta^{\frac{3}{2}} + m_{eff}\chi\delta\dot{\delta}$	$\frac{3}{2}$	1	Empirical value
Shäfer et al. [119]	$F_n = K\delta^{\frac{3}{2}} + \chi\delta\dot{\delta}$	$\frac{3}{2}$	1	Empirical value
Jankowski [120]	$F_n = K\delta^{\frac{3}{2}} + \chi\delta^{\frac{1}{2}}\dot{\delta}$	$\frac{3}{2}$	1	$2 \frac{-\ln e_r}{\sqrt{\pi^2 + (\ln e_r)^2}} \frac{K}{\delta_0}$
Zhiying-Qishao [113]	$F_n = K\delta^{\frac{3}{2}} + \chi\delta^{\frac{3}{2}}\dot{\delta}$	$\frac{3}{2}$	$\frac{3}{2}$	$\frac{3(1-c_r^2)e^{2(1-c_r)}}{4} \frac{K}{\delta_0}$
Bordbar-Hyppänen [121] Schwager-Poschel [122]	$F_n = K\delta^{\frac{3}{2}} + \chi\delta^{0.65}\dot{\delta}$	$\frac{3}{2}$	0.65	Empirical value
Gonthier et al. [103] Zhang-Sharf [123]	$F_n = K\delta^{\frac{3}{2}} + \chi\delta^{\frac{3}{2}}\dot{\delta}$	$\frac{3}{2}$	$\frac{3}{2}$	$\frac{1-c_r^2}{c_r} \frac{K}{\delta_0}$
Flores et al. [114]	$F_n = K\delta^{\frac{3}{2}} + \chi\delta^{\frac{3}{2}}\dot{\delta}$	$\frac{3}{2}$	$\frac{3}{2}$	$\frac{8(1-c_r)}{5c_r} \frac{K}{\delta_0}$
Gharib-Hurmuzlu [124]	$F_n = K\delta^{\frac{3}{2}} + \chi\delta^{\frac{3}{2}}\dot{\delta}$	$\frac{3}{2}$	$\frac{3}{2}$	$\frac{1}{c_r} \frac{K}{\delta_0}$
Brilliantov et al. [125]	$F_n = K\delta^{\frac{3}{2}} + \chi\delta^{\frac{1}{2}}\dot{\delta}$	$\frac{3}{2}$	$\frac{1}{2}$	$\frac{1}{K} \frac{(3\eta_2 - \eta_1)^2 (1-\nu)(1-2\nu)}{3\eta_2 + \eta_1 E\nu^2}$
Hu-Guo [115]	$F_n = K\delta^{\frac{3}{2}} + \chi\delta^{\frac{3}{2}}\dot{\delta}$	$\frac{3}{2}$	$\frac{3}{2}$	$\frac{3(1-c_r)}{2c_r} \frac{K}{\delta_0}$

is presented in Fig. 3 and for several contact-force models that define the analytical relation of the hysteresis-damping factor χ as a function of the coefficient of restitution. Every contact-force model is also compared to the Hertzian contact-force model that does not consider energy dissipation.

A force-indentation phase diagram of different contact-force models for different values of the coefficient of restitution are presented in Fig. 3 and compared with the Hertzian contact-force model that does not consider for energy dissipation. It is clear that when the coefficient of restitution is equal to 1 a force-indentation phase diagram is the same as Hertz for the contact models that have the hysteresis-damping factor χ that tend toward zero. Also, it is clear that if the coefficient of restitution approaches zero, the indentation-contact depth decreases and the magnitude of the contact force increases.

In Fig. 4 a normal component of the relative contact velocity relative to the contact-deformation depth is shown for different contact-force models. It is clear that at the start of the contact, when the compression phase begins, the relative normal contact velocity equals 0.3 m/s for all the contact models. Through contact evolution the compression phase ends when the relative normal contact velocity is equal to zero and the maximum contact-

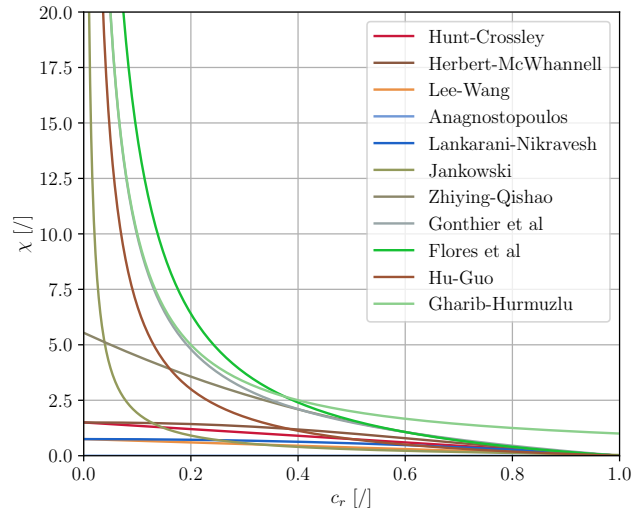


Fig. 2. Hysteresis-damping factor χ as a function of the coefficient of restitution c_r .

deformation depth is reached. At this point the restitution phase begins. At the end of the contact for the Hertzian contact model, which does not consider for energy dissipation during the contact process, the relative normal contact velocity is equal to -0.3 m/s. Different contact-force models that evaluate the energy dissipation with different hysteresis-damping models result in different values for the relative normal contact velocity at the contact finish that coincides with the end of the restitution phase.

Fig. 5 presents the evolution of the contact force in the normal direction over time for different contact-force models. For the Hertzian contact-force model the compression phase is symmetrical to the restitution phase, while for contact-force models that account for the energy dissipation during contact the restitution phase differs from the compression phase. It is clear that if the value of the coefficient of restitution decreases from 1 to 0, i.e., from a perfectly elastic to a perfectly plastic contact, the duration of the contact process also decreases for some contact-force models. Meanwhile, the magnitude of the contact force increases and the duration of the contact process does not change for these models, but the magnitude of the contact force decreases. Fig. 6 shows the velocity of the spheres i and j before, during and after the contact-impact event for different contact-force models at different values of the coefficient of restitution. Fig. 7 shows the kinetic energy of a multibody system assembled from two spheres before, during and after the contact-impact event for different contact-force models with the value of the coefficient of restitution from 0 to 1, i.e., from a perfectly plastic to a perfectly elastic contact situation. It is clear that the Hertzian contact-force model does not account for the energy dissipation during contact; therefore, the kinetic energy of the system after the contact is equal to the kinetic energy before the contact of the multibody system.

The output coefficient of restitution can be evaluated as [70]:

$$e_N = \frac{v_n}{v_0}, \quad (31)$$

where v_n is the relative normal contact velocity at the end of the contact and v_0 is the initial relative normal contact velocity (Newton's kinematic impact law). The coefficient of restitution is evaluated with Eq. (31) from the results of the numerical simulations for different contact-force models.

When performing numerical simulations the value of the coefficient of restitution, c_r , is set by the user input and used during the numerical simulations. On the other hand, the value of the coefficient of restitution can be evaluated from the numerical results in the post-processing stage. This evaluation can be made using Eq. (31) as the ratio of the relative contact velocity between the end and the beginning of the contact. In Table 2 a comparison between the evaluated values of the coefficient of restitution e_N , using Eq. (31), and the user-defined value of the coefficient of restitution c_r is presented for different contact-force models. The evaluated values of e_N are based on the numerical data presented in Fig. 4 and Fig. 6.

The effect of the coefficient of restitution on the loss of mechanical energy during the impact between two bodies for several contact-force models is shown in Fig. 8.

The time interval for the contact process is related to the value of the coefficient of restitution. The contact time for the different contact-force models relative to the contact time for the Hertzian contact model at different

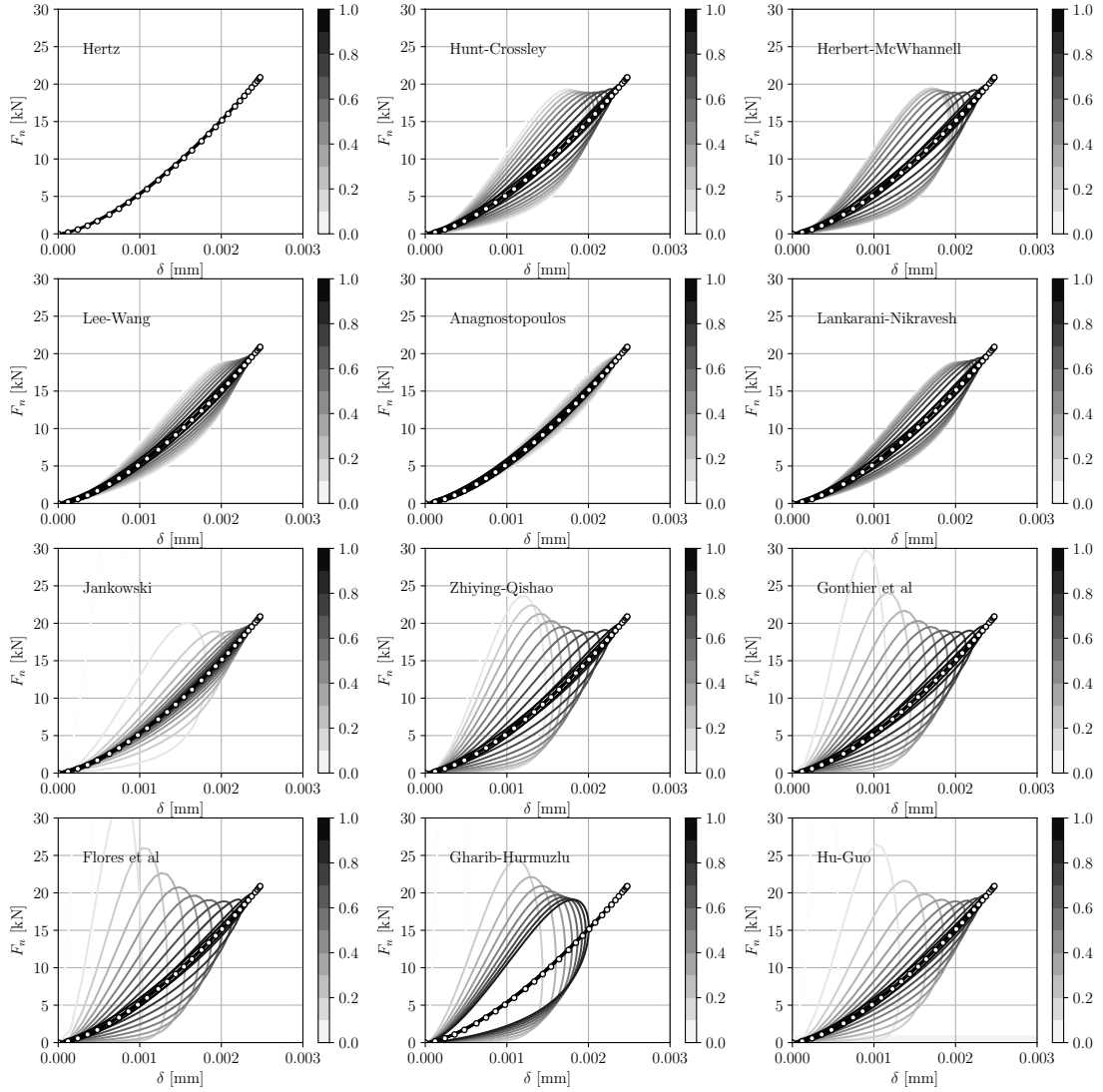


Fig. 3. Force-indentation relation for different contact-force models for a direct-central impact of two spheres and for different values of the coefficient of restitution.

values of the coefficient of restitution is presented in Fig. 9.

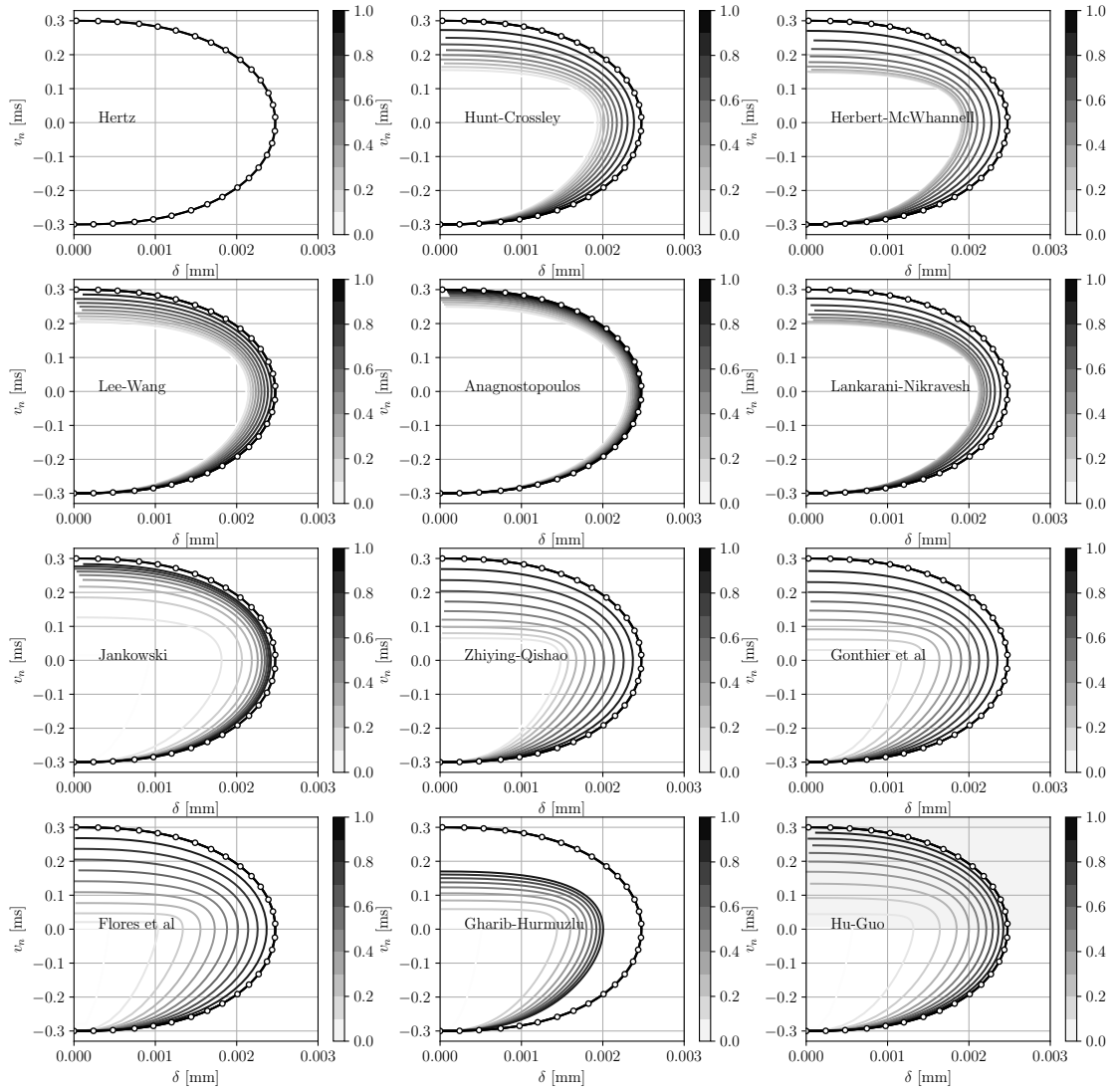


Fig. 4. Relative normal contact velocity vs. the deformation relation.

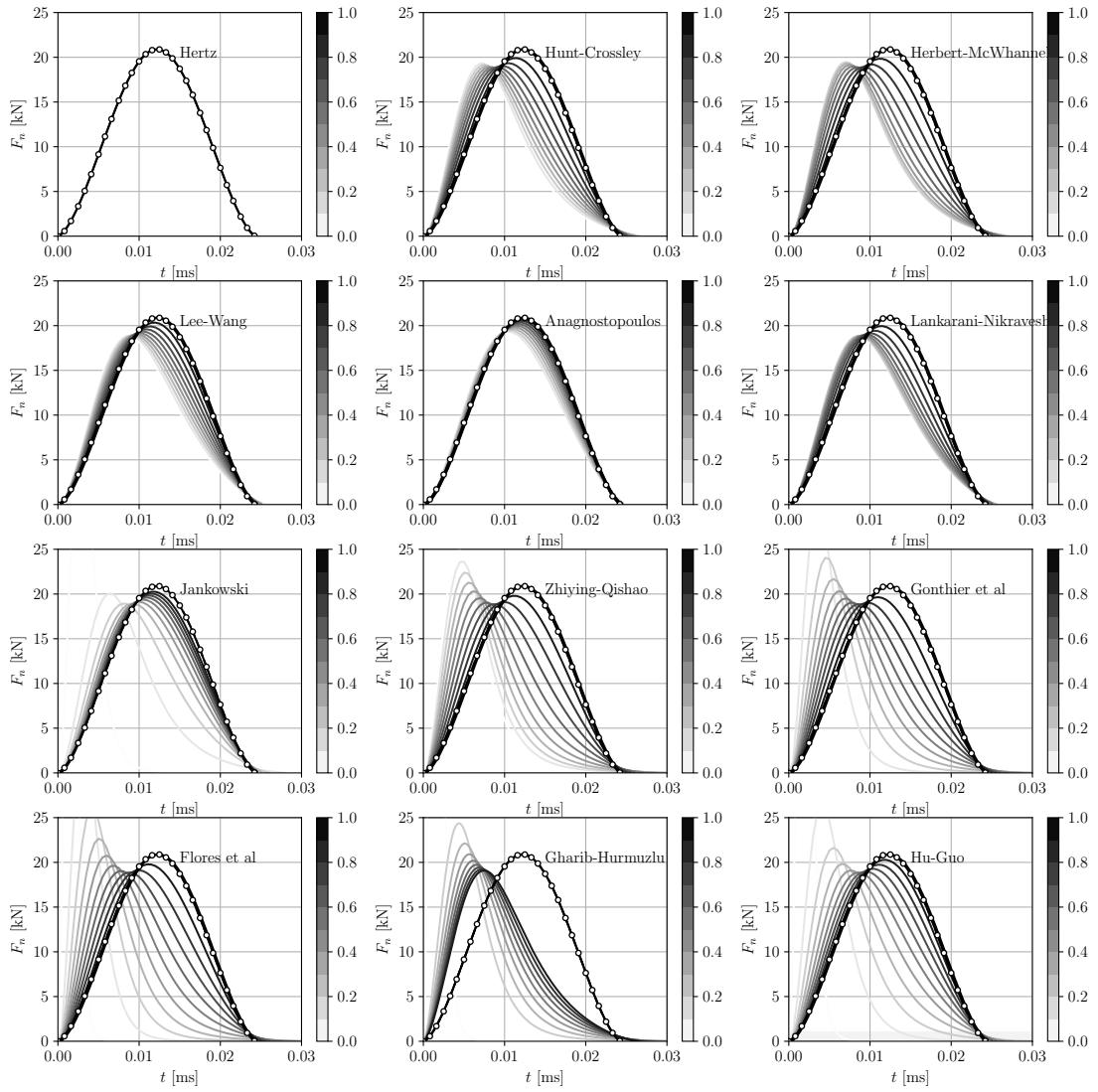


Fig. 5. Contact force during the contact-impact process.

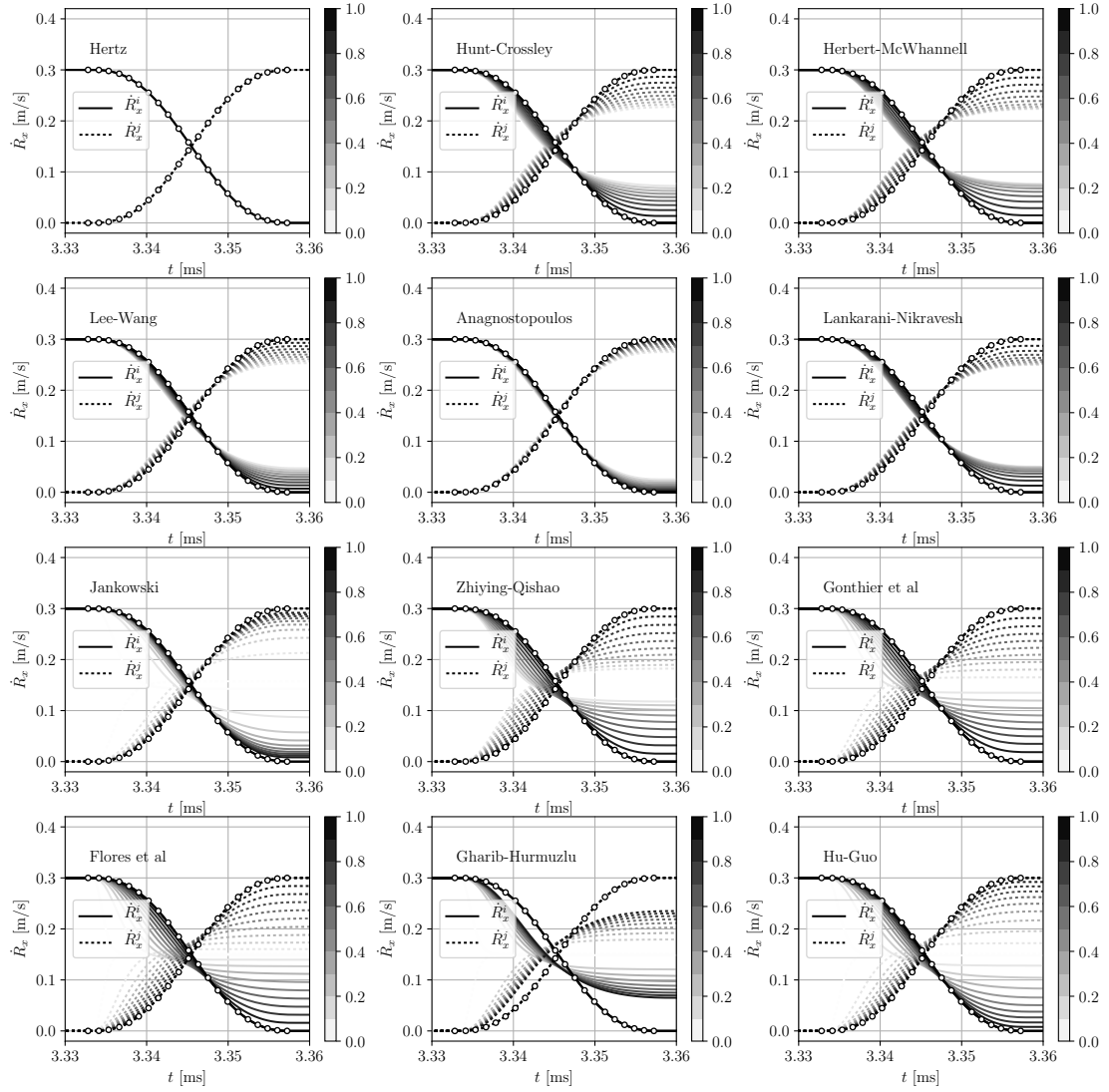


Fig. 6. Velocity of the spheres before, during and after the contact-impact event for different values of the coefficient of restitution.

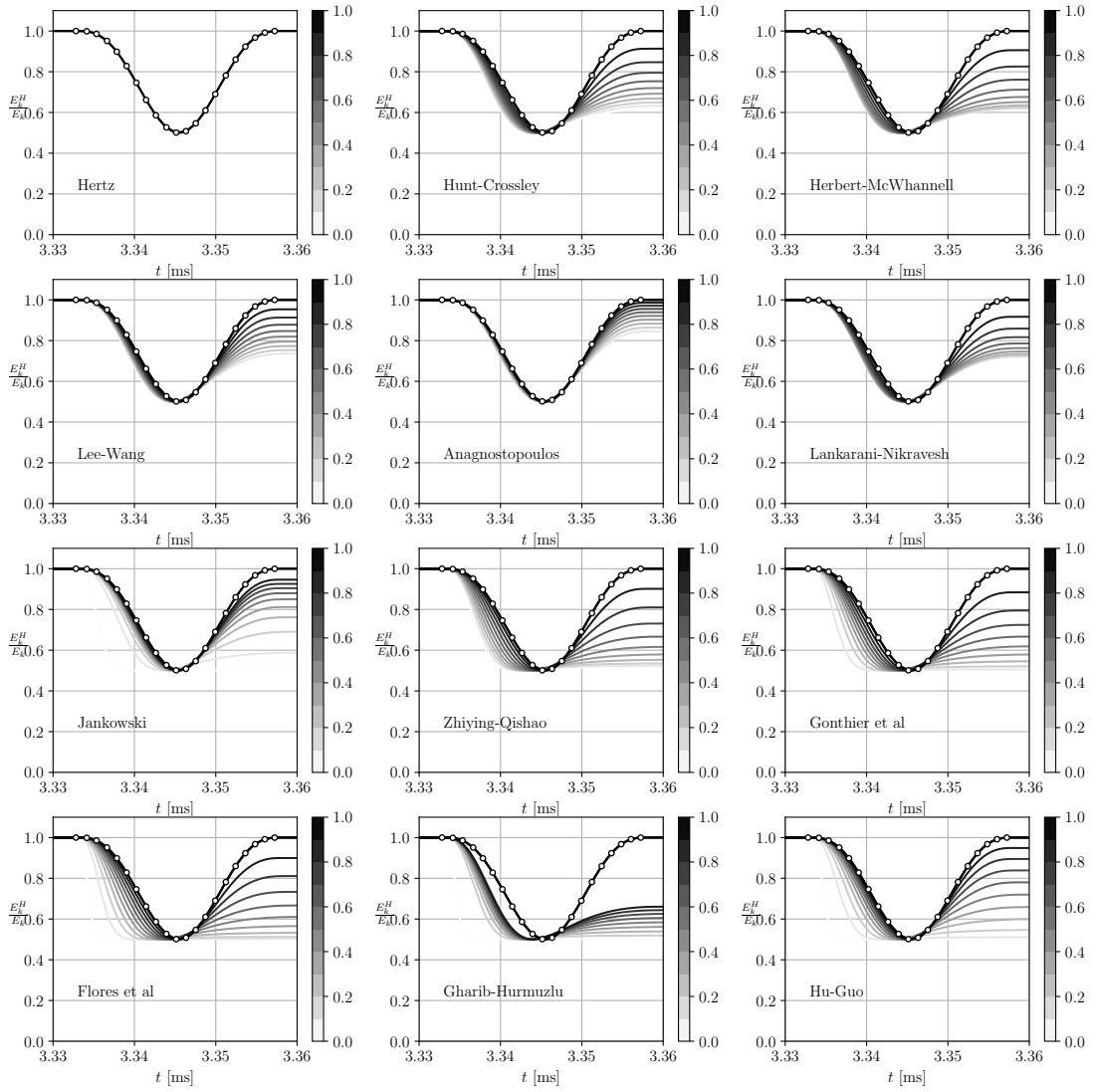


Fig. 7. Mechanical energy of a dynamical system over time during the contact-impact event for different coefficient of restitution relative to the Hertzian contact model.

Table 2

Evaluated values of the kinetic coefficient of restitution e_N compared to the user-defined values c_r .

Contact model	User-defined values of the coefficient of restitution - c_r										
	0.00	0.10	0.20	0.30	0.40	0.50	0.60	0.70	0.80	0.90	1.00
Hertz	1.00	1.00	1.00	1.00	1.00	1.00	1.00	1.00	1.00	1.00	1.00
Hunt-Crossley	0.49	0.52	0.55	0.58	0.62	0.66	0.71	0.77	0.83	0.91	1.00
Herbert-McWhannell	0.49	0.49	0.50	0.52	0.55	0.59	0.65	0.72	0.81	0.90	1.00
Lee-Wang	0.66	0.69	0.71	0.74	0.77	0.80	0.83	0.87	0.91	0.95	1.00
Anagnostopoulos	1.00	1.00	1.00	1.00	1.00	1.00	1.00	1.00	1.00	1.00	1.00
Lankarani-Nikravesh	0.66	0.67	0.67	0.68	0.70	0.73	0.76	0.80	0.85	0.91	1.00
Jankowski	0.07	0.44	0.63	0.74	0.80	0.85	0.89	0.91	0.94	0.96	1.00
Zhiying-Qishao	0.20	0.24	0.28	0.34	0.42	0.50	0.59	0.69	0.80	0.91	1.01
Gonthier et al	0.03	0.12	0.22	0.32	0.42	0.51	0.59	0.68	0.78	0.89	1.01
Flores et al	0.00	0.09	0.17	0.27	0.38	0.49	0.59	0.70	0.80	0.91	1.01
Gharib-Hurmuzlu	0.03	0.12	0.21	0.30	0.37	0.43	0.48	0.52	0.55	0.58	0.61
Hu-Guo	0.01	0.15	0.31	0.45	0.56	0.66	0.75	0.82	0.89	0.95	1.00

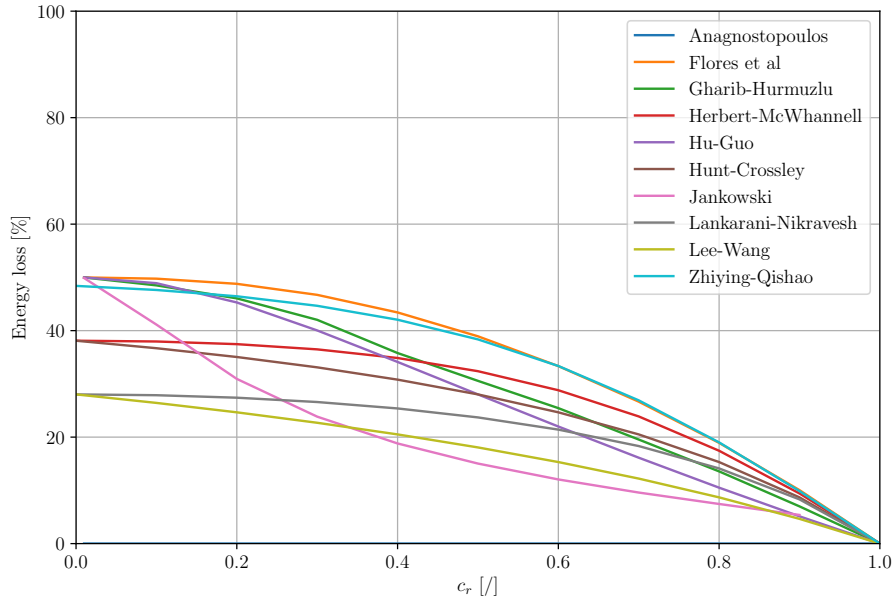


Fig. 8. Loss of mechanical energy versus coefficient of restitution for different contact models.

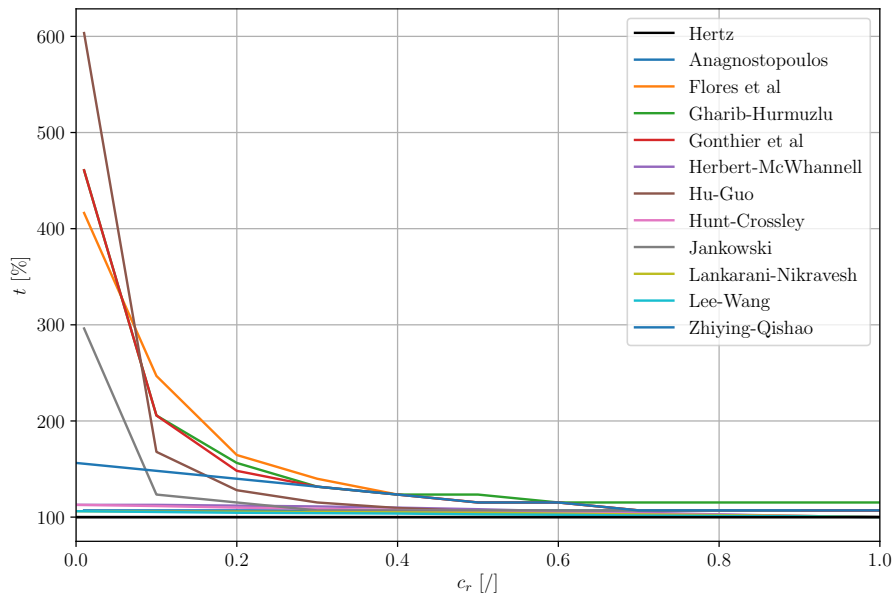


Fig. 9. Relative contact time relative to the Hertzian model versus the coefficient of restitution for different contact models.

4 Review of the cylindrical contact-force models

Most of the analytical cylindrical contact-force models, defining the relationship between the contact penetration and the applied contact force, that can be used for the internal or external contact between two cylindrical bodies, are based on the Hertzian pressure distribution [88, 89]. These models are all nonlinear as the penetration is presented as an implicit function of the contact force. There are three important drawbacks to these models [77]. First, (i) the contact force cannot be defined as an explicit function of the indentation, i.e., in a closed form, and this presents a problem when an iterative solution technique has to be used, i.e., a Newton-Rhapson algorithm [126], for each integration time step in the analysis of multibody dynamics [31, 127–129]. A typical internal cylindrical contact can also be used to model roller-bearing elements [130].

The Hertzian theory is based on an elastostatic theory that does not account for the energy dissipated during the contact-impact process. As a result, the Hertzian contact model cannot be used during the loading and unloading phases of the contact unless this is a quasi-static process and the contacting bodies have well-defined geometries. Furthermore, a contact-detection procedure must have available the information about any new contact deformation at the current and previous time step to successfully detect the start of the contact-impact event and to avoid any artificial energy gains in the multibody system [51]. As an iterative algorithm requires an initial guess about the contact indentation, a good and reasonable initial approximation at the current time step is to take the value of contact deformation calculated from the previous step as it is already evaluated, as implemented in the software code used in this paper [131]. Second, (ii) the contact models that are based on the Hertzian theory do not guarantee the correct value of the contact force, when the size of the contact area is about the same as the dimensions of the contact bodies, i.e., a conformal contact condition. The Hertzian theory is valid for the conditions in a nonconformal contact, where the dimensions of the contact area are small compared to the radii of the undeformed cylindrical bodies. Third, (iii) is the drawback related to the expressions that use a logarithmic function for the relationship between the contact force and the contact deformation, as the logarithmic function represents some of the mathematical and physical limitations on the internal contact analysis.

In the previous section the development of the general contact-force models together with the definitions of the hysteresis-damping factor are presented. Most of the presented cylindrical contact-force models in this section are an implicit function of the contact deformation δ and therefore require iterative solution techniques like a Newton-Rhapson algorithm for each integration time step. Another drawback is the lack of any energy dissipation, which can take place in two steps: firstly, a contact force is evaluated with a selected cylindrical contact-force model and, secondly an energy dissipation is included via the selected hysteresis-damping factor, as in [82, 86] for the Johnson model with energy dissipation.

The contact problem for the two cylindrical bodies with radii R_1 and R_2 can represent a revolute clearance joint assembled from a pin inside a cylindrical hole. Both bodies are made of isotropic material, where E_i is the Young's modulus and ν is the Poisson's ratio.

The key to solving the contact problems between two contacting cylinders is to obtain the area of the contact and the stress distribution. In Hertzian theory [88, 132] the contact area is approximated by a rectangle of width $2a$ aligned with the axes of the cylinders, which can be considered as the limiting case of an elliptical contact. The pressure distribution can be defined as a function of the variables a , the semi-width of the contact, and p_0 , the maximum pressure at the center of the contact width:

$$p(x) = p_0 \left(1 - \frac{x^2}{a^2} \right)^{\frac{1}{2}}, \quad (32)$$

where x is the distance of the point from the center of the contact plane.

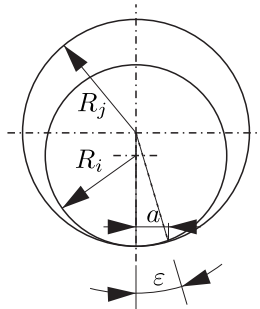


Fig. 10. Geometry of internal cylindrical contact - a revolute clearance joint.

The contact-force model for a cylindrical contact, developed by Hertz for the internal contact between two cylinders, defines the relationship between the depth of the contact deformation δ and the contact force per unit length f_n as:

$$\delta = \frac{2f_n}{\pi E^*} \left(\ln \left(\frac{\pi E^* \Delta R}{f_n} \right) - 1 \right), \quad (33)$$

where E^* is the modulus of elasticity of the contact, as the deformation of both bodies in contact must be considered, and is defined as [88]:

$$\frac{1}{E^*} = h_i + h_j, \quad (34)$$

where h_k ($k = i, j$) is defined using Eq. (3). In addition, ΔR is defined as:

$$\Delta R = R_i \pm R_j. \quad (35)$$

The definition of Eq.(33) can be found in [132]. In the case of an external contact Eq. (35) represents the sum of the radii of both cylinders and in the case of an internal contact Eq. (35) represents the difference between the radii of both cylinders and can be considered as the clearance for the revolute clearance joint. The Johnson model gives the best values when evaluating the contact force at the cylindrical contact in most engineering applications [77].

Based on Hertz's contact theory a new model was developed by Johnson that deals with the contact between two cylinders. This model defines the correlation between the depth of the contact deformation δ and the contact force per unit length f_n as [88]:

$$\delta = \frac{f_n}{\pi E^*} \left(\ln \left(\frac{4\pi E^* \Delta R}{f_n} \right) - 1 \right), \quad (36)$$

Eq. (36) can be used in the case of an internal or external contact between two cylinders.

In the book Formulas for Stress and Strain [133] a contact model developed by Radzimovsky is presented. The Radzimovsky model defines the relationship for the distance between the centers for the contact between external cylinders, i.e., the indentation δ and the normal contact force per unit length with an expression [134]:

$$\delta = \frac{f_n}{\pi E^*} \left(\frac{2}{3} + \ln \left(\frac{4R_i}{b} \right) + \ln \left(\frac{4R_j}{b} \right) \right), \quad (37)$$

where, in the case of cylinders with different materials, the parameter b is evaluated according to:

$$b = 1.60 \left(\frac{f_n R}{E^*} \right)^{\frac{1}{2}}, \quad (38)$$

where E^* is the composite modulus and evaluated with Eq. (34). In the case of similar materials the parameter b is evaluated as:

$$b = 2.15 \left(\frac{f_n R}{E^*} \right)^{\frac{1}{2}} \quad (39)$$

and the parameter R defines the relative curvature of the contact and is defined as:

$$R = \frac{R_i R_j}{R_i \pm R_j} = \frac{R_i R_j}{\Delta R}, \quad (40)$$

where the sign \pm depends on the type of contact, i.e., $(-)$ for an internal and $(+)$ for an external contact. Eq. (40) can be used to rewrite Eq. (37) in the form suggested by Johnson as [88]:

$$\delta = \frac{f_n}{\pi E^*} \left(\frac{2}{3} + \ln \left(\frac{8\Delta R E^*}{b_0^2 f_n} \right) \right), \quad (41)$$

where the value of the parameter b_0 depends on the material properties of the colliding cylinders, i.e., it has a value of 1.60 for different materials or 2.15 for similar materials.

Based on Hertz's contact theory an alternative contact-force model was developed by Goldsmith for the case of an internal contact between two cylinders. The Goldsmith model relates the depth of the contact deformation δ and the contact force F_n using the following expression [48]:

$$\delta = F_n \left(\frac{h_i + h_j}{L} \right) \left(\ln \left(\frac{L^m}{F_n R (h_i + h_j)} \right) + 1 \right), \quad (42)$$

where R is the relative curvature of the contact and is defined by Eq. (35), L is the contact length and m is the power factor. In the case when the value of $m = 1$, Eq. (42) guarantees the compliance of the units. The contact-force model proposed by Goldsmith was initially developed for an internal contact, although it is also possible to use it for an external contact, but extra caution is needed for the correct use of Eq. (40). In the case of an internal contact, the difference between the radii of the cylinders is used and in the case of an external contact the sum of the radii is used.

Based on the contact theory developed by Hertz and the contact model proposed by Goldsmith the authors Dubowsky and Freudenstein presented their contact-force model for the internal cylindrical contact between two cylinders [135]:

$$\delta = F_n \left(\frac{h_i + h_j}{L} \right) \left(\ln \left(\frac{L^m (R_i - R_j)}{F_n R_i R_j (h_i + h_j)} \right) + 1 \right), \quad (43)$$

where L is the length of the contact and the power factor m is equal to 3. A comparative study between these two expressions was carried out by Flores et al. [136], in which the solutions corresponding to the time variation of indentation, the normal contact force, and the force-indentation ratio presented by these two models are researched.

The model developed by Johnson [88], Eq. (36), is one of the most popular for defining the relationship between the indentation and the contact force, and it is also the basis for the expression developed by the ESDU 78035 Tribology Series for journal-bearing applications [137]:

$$\delta = F_n \left(\frac{h_i + h_j}{L} \right) \left(\ln \left(\frac{4L (R_i - R_j)}{F_n (h_i + h_j)} \right) + 1 \right). \quad (44)$$

The ESDU-78035 model is named after the publisher *Engineering Sciences Data Unit*, which acts as a consultant in different fields of engineering.

In [132] Liu et al. presented the drawbacks of the contact models developed by Hertz and Persson. They suggested that the Hertzian model can be used for larger values of clearance and smaller contact forces, while the Persson model can be used for smaller clearance values. Based on numerical FEM results Liu et al. [132] introduced the following explicit relationship between the contact force F_n and the depth of the deformation δ :

$$F_n = \frac{1}{2} \pi \delta E^* \left(\frac{\delta}{2(\Delta R + \delta)} \right)^{\frac{1}{2}}. \quad (45)$$

If the dissipation element in the general contact law proposed by Lankarani and Nikravesh [71,83] is omitted, then the deformation depth can be evaluated as:

$$\delta = \left(\frac{3F_n}{4E^* R^{\frac{1}{2}}} \right)^{\frac{1}{n}}. \quad (46)$$

In the case of a contact between two spheres the value of the power factor n is equal to 1.5. Assuming that the contact force is evenly distributed along the length of the cylinders and that the boundary affect is ignored then Eq. (46) can be used for the contact between two cylinders with the value of the power factor n being between 1 and 1.5 [101].

An enhanced cylindrical contact-force model was developed by Pereira et al. to overcome the shortcomings of the basic cylindrical contact-force models that use an implicit function of the contact force F_n and the contact deformation δ and also lack the energy dissipation.

Pereira et al. proposed an enhanced cylindrical contact-force model based on the Johnson model [83] and a complementary finite-element analysis valid for the internal and external cylindrical contacts. Their model also overcomes the computational complexity as the relationship between the depth of the contact deformation δ and the contact force F_n is defined explicitly as [86]:

$$F_n = \frac{(a\Delta R + b) L E^*}{\Delta R} \delta^n \left(1 + \frac{3}{4} \frac{\dot{\delta}}{\dot{\delta}_0} (1 - c_r^2) \right), \quad (47)$$

Table 3

Values for an enhanced cylindrical contact-force model.

	internal contact	external contact
a	0.965	0.39
b	0.0965	0.85
n	$Y\Delta R^{-0.005}$	1.094

where the parameters are the same as in Eq. (18) and the values of the parameters a , b and n are listed in Table 3.

In the case of an internal contact the value of the parameter n is not constant; therefore, the following expression is used to evaluate it:

$$Y = \begin{cases} 1.51 \ln(1000\Delta R)^{-0.151}, & \text{if } \Delta R \in [0.005, 0.34954] \text{ mm,} \\ 0.0151\Delta R + 1.151, & \text{if } \Delta R \in [0.34954, 10.0] \text{ mm,} \end{cases} \quad (48)$$

and the parameter ΔR is evaluated with Eq. (35). It should be emphasized that all the parameters in this model have units in mm.

As can be seen in Eq. (47), an expression for the hysteresis-damping factor defined by Lankarani and Nikravesh is used to include the energy dissipation during the contact process. Similarly, an arbitrary definition of the hysteresis-damping factor, defined in Section 2, can be used to include the energy dissipation as presented in the example of a contact between two spheres (see Section 3). Similarly, a hysteresis-damping factor can be used with an arbitrary cylindrical contact-force model, as presented in Section 6.

Table 4

Cylindrical contact-force models.

Contact force model	Formulation	Notes
Hertz [81]	$\delta = \frac{2f_n}{\pi E^*} \left(\ln \left(\frac{\pi E^* \Delta R}{f_n} \right) - 1 \right)$	
Radzimovsky [134]	$\delta = \frac{f_n}{\pi E^*} \left(\frac{2}{3} + \ln \left(\frac{4R_i}{b} \right) + \ln \left(\frac{4R_j}{b} \right) \right)$	
Goldsmith [48]	$\delta = F_n \left(\frac{h_i+h_j}{L} \right) \left(\ln \left(\frac{L^m}{F_n R (h_i+h_j)} \right) + 1 \right)$	$m = 1$
Dubowsky-Freudenstein [135]	$\delta = F_n \left(\frac{h_i+h_j}{L} \right) \left(\ln \left(\frac{L^m (R_i-R_j)}{F_n R_i R_j (h_i+h_j)} \right) + 1 \right)$	$m = 3$
Lankarani-Nikravesh [71]	$\delta = \left(\frac{3F_n}{4E^* R^{\frac{1}{2}}} \right)^{\frac{1}{n}}$	
ESDU-78035 [137]	$\delta = F_n \left(\frac{h_i+h_j}{L} \right) \left(\ln \left(\frac{4L(R_i-R_j)}{F_n (h_i+h_j)} \right) + 1 \right)$	
Johnson [88]	$\delta = \frac{f_n}{\pi E^*} \left(\ln \left(\frac{4\pi E^* \Delta R}{f_n} \right) - 1 \right)$	
Liu et al. [132]	$F_n = \frac{1}{2} \pi \delta E^* \left(\frac{\delta}{2(\Delta R + \delta)} \right)^{\frac{1}{2}}$	
Pereira et al. [86]	$F_n = \frac{(a\Delta R + b)LE^*}{\Delta R} \delta^n \left(1 + \frac{3}{4} \frac{\delta}{\delta_0} (1 - c_r^2) \right)$	
Persson [138]	$F_n = \frac{E^* \Delta R \pi (b^2 + 1) b^2}{2(\Delta R + \delta)}$	$b = \tan \left(\frac{\varepsilon}{2} \right), \varepsilon = \arccos \left(\frac{\Delta R}{\Delta R + \delta} \right)$

5 Comparison of the cylindrical contact-force models

To compare the evolution of the contact force of the presented contact-force models for a cylindrical contact a simple multibody system assembled from two cylinders, presented in Fig. 11, is used. The properties of the multibody system are listed in Table 5.

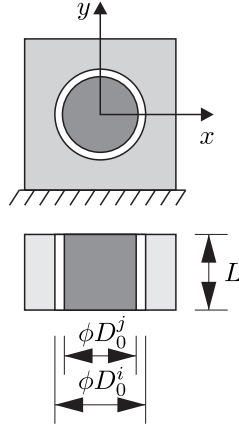


Fig. 11. An internal cylindrical contact.

Table 5

Properties of the multibody system.

parameter	i	j
m [kg]	37.6×10^{-3}	8.29×10^{-3}
J [kg m ²]	3.01×10^{-6}	9.36×10^{-8}
$R_0 \left(\frac{D_0}{2}\right)$ [m]	5×10^{-3}	4.75×10^{-3}
L [m]	15×10^{-3}	15×10^{-3}
\mathbf{q}_0 [m, m, deg]	[0, 0, 0]	[0, 0, 0]
$\dot{\mathbf{q}}_0$ [m, m, deg]/s	[0, 0, 0]	[0, -0.2, 0]
E [Pa]	2.1×10^{11}	2.1×10^{11}
ν [/]	0.3	0.3

Fig. 12 presents a comparison of the contact force per unit length for cylindrical contact-force models without energy dissipation relative to the contact deformation depth. It is clear that the maximum value of the contact force and the maximum value of the penetration depth for different cylindrical contact-force models are very different. These maximum values of the contact force and the contact penetration depth are in an inverse relationship when compared for different models.

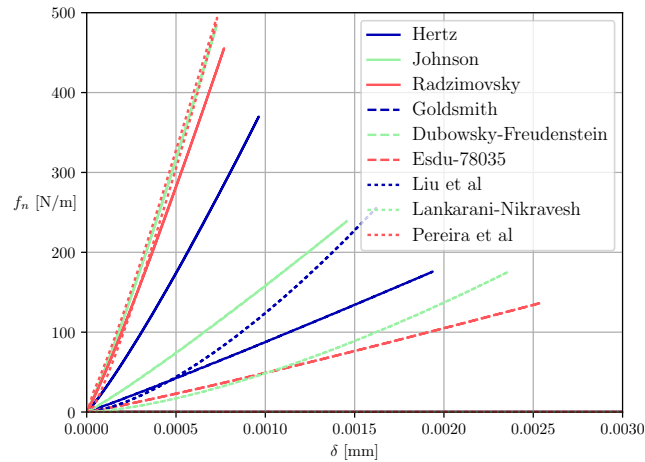


Fig. 12. Contact force based on the depth of the contact deformation for an internal cylindrical contact.

Fig. 13 has a comparison of the contact force per unit length of a cylindrical contact for the presented cylindrical contact-force models without energy dissipation relative to simulation time. It is clear that for a shorter duration of the contact-impact process, the peak value of the contact force is larger and in the case of

longer durations of contact-impact process the peak value of the contact force is smaller. Because there is no energy-dissipation included, the evolution of the contact force over time is symmetrical in the compression and restitution phases, observed from the point of the maximum value of the contact force.

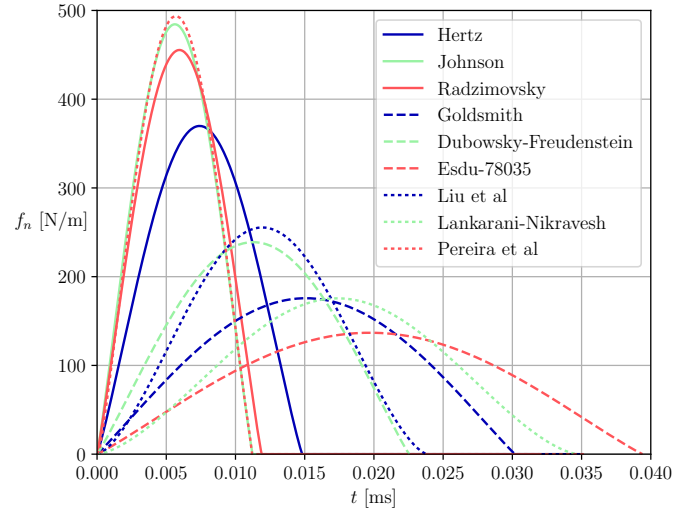


Fig. 13. Contact force during the contact-impact process for an internal cylindrical contact.

6 Discussion

The synthetic numerical example presented in Sec. 5 is extended here with dissipation elements. For a contact model that defines an implicit relationship between the contact force and the contact deformation, an energy dissipation is added in two steps: in the first step the contact force is evaluated with an iterative technique, such as the Newton-Rhaphson method, and in the second step hysteresis damping is used to include the energy dissipation during the contact process for each integration time step. In the numerical example a Lankarani-Nikravesh hysteresis damping is used, Eq. (17). An enhanced cylindrical contact-force model defines the explicit relationship between the deformation depth and the contact force; therefore, only one evaluation of Eq. (47) is required for each integration time step, and it also includes an expression for the hysteresis damping of Lankarani-Nikravesh.

In Fig. 14 a comparison of the presented cylindrical contact force models is shown. The models compared are: Hertz (cylindrical), Johnson, Radzimovsky, Goldsmith, Dubowsky-Freudenstein, ESDU-78035, Liu et al., Lankarani-Nikravesh (cylindrical) and Pereira et al. All of the models represent the relationship between the contact force and the depth of the contact deformation as an implicit function, except for the model of Pereira et al., which defines the relationship between the contact force and the depth of the contact deformation explicitly. The hysteresis damping of Lankarani-Nikravesh and the coefficient of restitution value of 0.7 are used. The parameters and their values for the numerical example are equal to the one used in Section 5, see Table 5.

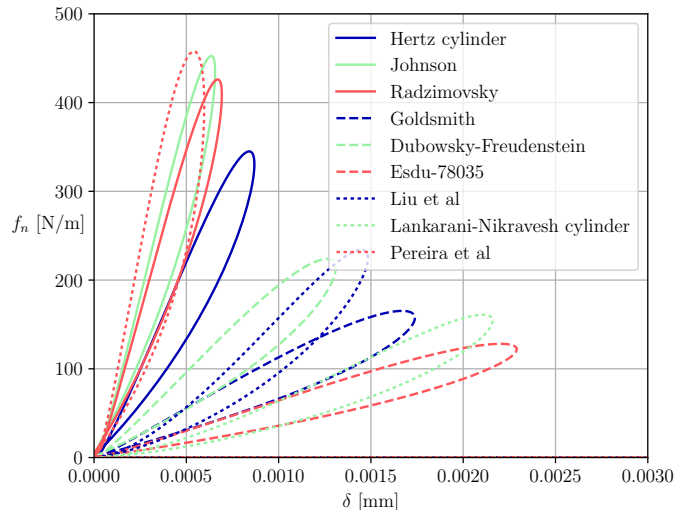


Fig. 14. Contact force based on the depth of the contact deformation for an internal cylindrical contact with energy dissipation.

In Fig. 15 the comparison of the contact force for a cylindrical contact with energy dissipation is presented. When compared to the contact force presented in Fig. 13, it is clear that without energy dissipation the contact force in the compression shape is symmetrical with the restitution phase, but when the hysteresis damping is used the force in the compression phase is different from the restitution phase.

When dealing with the contact-impact events great care has to be taken with the selection of the contact-force model and suitable hysteresis damping. To guarantee the quality of the numerical results an experimental validation is recommended [84].

The contact models presented in this paper are implemented in a custom-written, open-source, computer software code *DyS* that is publicly available [84]. The software automatically builds the equations of motion for an arbitrary dynamical system and solves them numerically using appropriate numerical methods.

The relative error of the evaluated coefficient of restitution, presented in Table 2, depending on the user-defined value of the coefficient of restitution is presented in Fig. 16 for different contact-force models. The relative error between the evaluated value of the coefficient of restitution, e_N , and the user-defined input value of the coefficient of restitution, c_r , is evaluated as:

$$Rel. Error = \frac{|c_r - e_N|}{c_r}. \quad (49)$$

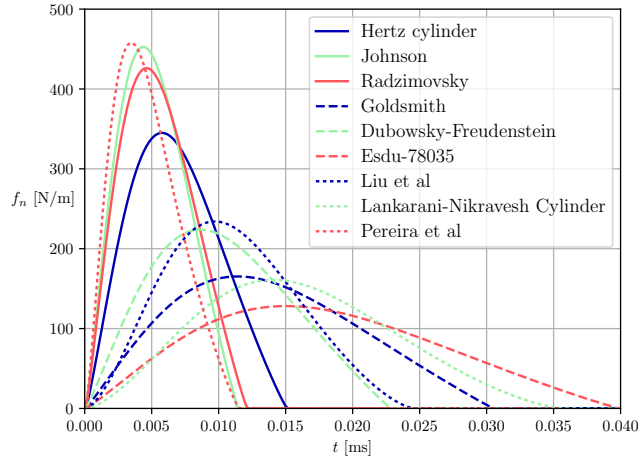


Fig. 15. Contact force during the contact-impact process for an internal cylindrical contact with energy dissipation.

It is clear that the relative error of the coefficient of restitution is small for the majority of the contact-force models, where the value of the coefficient of restitution is greater than 0.5. Also, it is clear that the contact-force models of Gonthier et al., Flores et al., Gharib-Hurmuzlu and Hu-Guo have small relative errors between the input values of the of restitution and the evaluated values, based on the relative contact velocities in the normal direction before and after the contact-impact event.

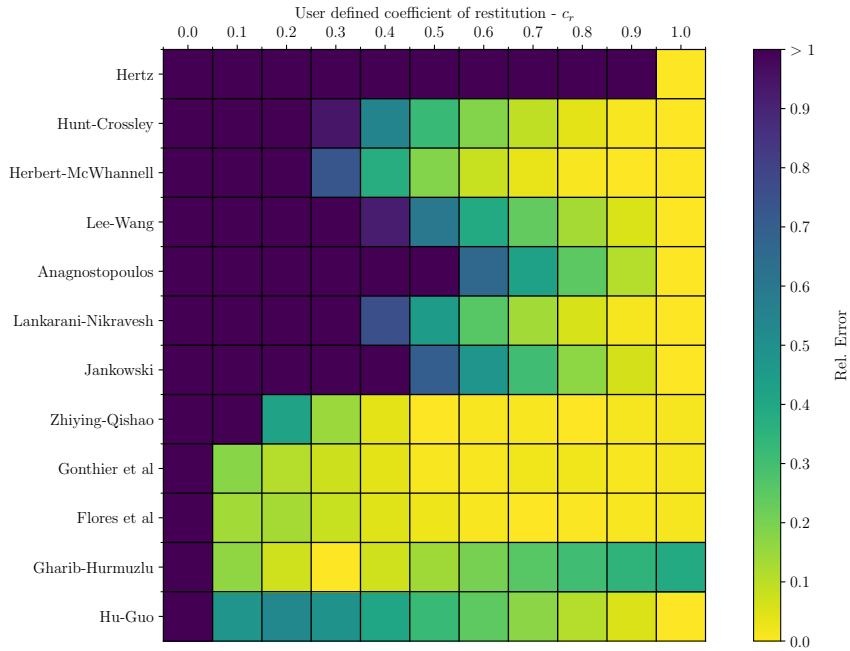


Fig. 16. Relative error of the evaluated coefficient of restitution, e_N , if compared to the user-defined value, c_r .

7 Conclusions

A review and comparison of continuous contact-force models that can be used when modeling a general or cylindrical contact between the bodies is described. In the group of general contact-force models (point contact) 20 different contact-force models are listed, and numerical simulations are performed with a dozen of these contact-force models. When comparing the dynamical response of a multibody system, i.e., a body's (sphere) velocity before, during and after the contact, it is clear that different contact force-models with a selected value of the coefficient of restitution have a great impact on the dynamical response. Furthermore, the dissipated energy of the dynamical system varies significantly and this difference increases when the value of the coefficient of restitution nears zero. The research focus is also on the differences in the energy dissipation due to the coefficient of restitution and the duration of the contact. In addition, these attributes are compared to the Hertzian contact-force model. In the group of cylindrical contact-force models (line contact) the following models are compared: Hertz (cylindrical), Johnson, Radzimovsky, Goldsmith, Dubowsky-Freudenstein, ESDU-78035, Liu et al., Lankarani-Nikravesh (cylindrical) and Pereira et al.

The comparison of the hysteresis-damping models depending on the coefficient of restitution is presented and the effects of the hysteresis damping on the contact force, the mechanical energy and the velocity are shown. A comparison of the evolution of the contact force during the contact-impact process for the presented general contact-force models is made. The effect of hysteresis damping is compared for the presented cylindrical contact-force models in the discussion. Also, the difference between the contact force for the cylindrical contact force without energy dissipation and with energy dissipation, including the hysteresis damping, is presented.

The magnitude of contact force generally decreases, while the value of the coefficient of restitution goes from value 1 to value 0, i.e., from perfectly elastic contact to perfectly plastic contact, but the duration of the contact-impact process is constant, see Fig. 5.

Based on the evaluation of the kinetic coefficient of restitution with Eq. (31) from numerical results of velocities before and after contact-impact process it is clear from Fig. 16 that for five contact force models (Zhiying-Qishao, Gonthier et al., Flores et al., Gharib-Hurmuzlu and Hu-Guo) there is a good agreement between user-defined value and the evaluated one on the whole interval, i.e., from 0 to 1. On the other hand, for the six contact force models (Hunt-Crossley, Herbert-McWhannell, Lee-Wang, Anagnostopoulos, Lankarani-Nikravesh and Jankowski) there is a good agreement for values of the coefficient of restitution greater than 0.5, therefore it is wise to use this models on the interval from 0.5 to 1 - from semi-elasto-plastic contact to perfectly elastic contact.

Acknowledgment

The authors acknowledge the partial financial support from the Slovenian Research Agency (research core funding No. P2-0263).

References

- [1] Elias Dimitrakopoulos, Andreas J Kappos, and Nicos Makris. Dimensional analysis of yielding and pounding structures for records without distinct pulses. *Soil Dynamics and Earthquake Engineering*, 29:1170–1180, 2009.
- [2] Elias G. Dimitrakopoulos. Analysis of a frictional oblique impact observed in skew bridges. *Nonlinear Dynamics*, 60:575–595, 2010.
- [3] Gregory L Cole, Rajesh P Dhakal, and Fred M Turner. Building pounding damage observed in the 2011 Christchurch earthquake. *Earthquake Engineering and Structural Dynamics*, 41(August 2011):893–913, 2012.
- [4] Gerald Ristow. Simulating Granular Flow with Molecular Dynamics. *J. Phys. I*, 2(6):649, 1992.
- [5] Selçuk Erkaya and Ibrahim Uzmay. A neural-genetic (NN-GA) approach for optimising mechanisms having joints with clearance. *Multibody System Dynamics*, 20(1):69–83, 2008.
- [6] Adel Izadbakhsh, John McPhee, and Stephen Birkett. Dynamic Modeling and Experimental Testing of a Piano Action Mechanism With a Flexible Hammer Shank. *Journal of Computational and Nonlinear Dynamics*, 3(July):031004, 2008.

- [7] Paulo Flores and Hamid M. Lankarani. Spatial rigid-multibody systems with lubricated spherical clearance joints: modeling and simulation. *Nonlinear Dynamics*, 60(1-2):99–114, 2009.
- [8] Paulo Flores, Margarida MacHado, Miguel T. Silva, and Jorge M. Martins. On the continuous contact force models for soft materials in multibody dynamics. *Multibody System Dynamics*, 25(3):357–375, 2011.
- [9] Zhe Wang, Qiang Tian, and Haiyan Hu. Dynamics of spatial rigid-flexible multibody systems with uncertain interval parameters. *Nonlinear Dynamics*, 84(2):527–548, 2016.
- [10] Francesco Mocera and Andrea Nicolini. Multibody simulation of a small size farming tracked vehicle. *Procedia Structural Integrity*, 8:118–125, 2018.
- [11] Ahmed A Shabana, Khaled E Zaazaa, José L Escalona, and Jalil R Sany. Development of elastic force model for wheel/rail contact problems. *Journal of Sound and Vibration*, 269(1-2):295–325, 2004.
- [12] Joao Pombo, Jorge Ambrósio, Manuel Pereira, Roger Lewis, Rob Dwyer-Joyce, Caterina Ariaudo, and Naim Kuka. A study on wear evaluation of railway wheels based on multibody dynamics and wear computation. *Multibody System Dynamics*, 24(3):347–366, 2010.
- [13] José L Escalona and Javier F Aceituno. Multibody simulation of railway vehicles with contact lookup tables. *International Journal of Mechanical Sciences*, 2018.
- [14] Luis Baeza, David J Thompson, Giacomo Squicciarini, and Francisco D Denia. Method for obtaining the wheel–rail contact location and its application to the normal problem calculation through ‘CONTACT’. *Vehicle System Dynamics*, 0(0):1–13, 2018.
- [15] H. Kh Beheshti and H. M. Lankarani. A simplified test methodology for crashworthiness evaluation of aircraft seat cushions. *International Journal of Crashworthiness*, 11(1):27–35, 2006.
- [16] Luís Sousa, Paulo Veríssimo, and Jorge Ambrosio. Development of generic multibody road vehicle models for crashworthiness. *Multibody System Dynamics*, 19(1-2):133–158, 2007.
- [17] M Guida, A Manzoni, A Zuppari, F Caputo, F Marulo, and A De Luca. Development of a multibody system for crashworthiness certification of aircraft seat. *Multibody System Dynamics*, 1 2018.
- [18] Paula C. Silva, Miguel T. Silva, and Jorge M. Martins. Evaluation of the contact forces developed in the lower limb/orthosis interface for comfort design. *Multibody System Dynamics*, 24(3):367–388, 2010.
- [19] Ahmed A. Shabana, Florentina M. Gantoi, and Michael A. Brown. Integration of finite element and multibody system algorithms for the analysis of human body motion. *Procedia IUTAM*, 2:233–240, 2011.
- [20] Ivan Argatov. Development of an asymptotic modeling methodology for tibio-femoral contact in multibody dynamic simulations of the human knee joint. *Multibody System Dynamics*, 28(1-2):3–20, 2012.
- [21] Ehsan Askari, Paulo Flores, Danè Dabirrahmani, and Richard Appleyard. Study of the friction-induced vibration and contact mechanics of artificial hip joints. *Tribology International*, 70:1–10, 2014.
- [22] David Ingram, Christoph Engelhardt, Alain Farron, Alexandre Terrier, and Philippe Müllhaupt. Modelling of the human shoulder as a parallel mechanism without constraints. *Mechanism and Machine Theory*, 100:120–137, 2016.
- [23] Huipeng Chen, Varun Bollapragada, Teawung Kim, Bingbing Nie, Gwansik Park, and Jeff R. Crandall. Improvement of lateral shoulder impact response of a multi-body pedestrian model. *International Journal of Crashworthiness*, 8265(November), 2016.
- [24] Ali Zeighami, Rachid Aissaoui, and Raphael Dumas. Knee medial and lateral contact forces in a musculoskeletal model with subject-specific contact point trajectories. *Journal of Biomechanics*, 69:138–145, 3 2018.
- [25] D W Marhefka and D E Orin. A compliant contact model with nonlinear damping for simulation of robotic systems. *Systems, Man and Cybernetics, Part A: Systems and Humans, IEEE Transactions on*, 29(6):566–572, 11 1999.
- [26] Diederik Verscheure, Inna Sharf, Herman Bruyninckx, Jan Swevers, and Joris De Schutter. Identification of contact parameters from stiff multi-point contact robotic operations. *International Journal of Robotics Research*, 29(4):367–385, 2010.

- [27] Shu Sheng Bi, Xiao Dong Zhou, and Dan B. Marghitu. Impact modelling and analysis of the compliant legged robots. *Proceedings of the Institution of Mechanical Engineers, Part K: Journal of Multi-body Dynamics*, 226(2):85–94, 2012.
- [28] Mohui Jin and Xianmin Zhang. A new topology optimization method for planar compliant parallel mechanisms. *Mechanism and Machine Theory*, 95:42–58, 2016.
- [29] Engin Tanik. Analysis and design of an underactuated compliant five-bar mechanism. *Mechanism and Machine Theory*, 102:123–134, 2016.
- [30] Giuseppe Quaglia and Matteo Nisi. Design of a self-leveling cam mechanism for a stair climbing wheelchair. *Mechanism and Machine Theory*, 112:84–104, 2017.
- [31] Piyu Wang and Qingsong Xu. Design and modeling of constant-force mechanisms: A survey. *Mechanism and Machine Theory*, 119:1–21, 2018.
- [32] Selçuk Erkaya. Experimental investigation of flexible connection and clearance joint effects on the vibration responses of mechanisms. *Mechanism and Machine Theory*, 121:515–529, 2018.
- [33] Yang Liu, Joseph Páez Chávez, Ekaterina Pavlovskaja, and Marian Wiercigroch. Analysis and control of the dynamical response of a higher order drifting oscillator. *Proceedings of the Royal Society of London A: Mathematical, Physical and Engineering Sciences*, 474(2210), 2018.
- [34] Yulin Jin, Zhenyong Lu, Rui Yang, Lei Hou, and Yushu Chen. A new nonlinear force model to replace the Hertzian contact model in a rigid-rotor ball bearing system. *Applied Mathematics and Mechanics (English Edition)*, 39(3):365–378, 2018.
- [35] Farzin Montazersadgh and Mehran Mobrem. Structural Analysis Methodology for Space Deployable Structures using Multi-body Dynamic Analysis Solver. *2018 AIAA Modeling and Simulation Technologies Conference*, (January):1–10, 2018.
- [36] Oliver Maier, Benedikt Györfi, Jürgen Wrede, and Roland Kasper. Design and validation of a multi-body model of a front suspension bicycle and a passive rider for braking dynamics investigations. *Multibody System Dynamics*, 42(1):19–45, 2018.
- [37] Ahmed A. Shabana. *Computational dynamics*. Wiley, 2001.
- [38] Paulo Flores, Jorge Ambrosio, Claro C. J. Pimenta, and Hamid M. Lankarani. *Kinematics and Dynamics of Multibody Systems with Imperfect Joints*, volume 34 of *Lecture Notes in Applied and Computational Mechanics*. Springer, 2008.
- [39] Christian Klinger. Failures of cranes due to wind induced vibrations. *Engineering Failure Analysis*, 43:198–220, 2014.
- [40] Y. Q. Li, X. L. Gao, S. E. Horner, and J. Q. Zheng. Analytical models for the impact of a solid sphere on a fluid-filled spherical shell incorporating the stress wave propagation effect and their applications to blunt head impacts. *International Journal of Mechanical Sciences*, 130:586–595, 2017.
- [41] Uroš Proso, Janko Slavič, and Miha Boltežar. Vibration-fatigue damage accumulation for structural dynamics with non-linearities. *International Journal of Mechanical Sciences*, 106:72–77, 2016.
- [42] Andre T. Beck and Robert E. Melchers. Overload failure of structural components under random crack propagation and loading - A random process approach. *Structural Safety*, 26(4):471–488, 2004.
- [43] Shiyuan Luo, Dahu Zhu, Lin Hua, Dongsheng Qian, and Sijie Yan. Numerical analysis of die wear characteristics in hot forging of titanium alloy turbine blade. *International Journal of Mechanical Sciences*, 123:260–270, 2017.
- [44] Ahmed A. Shabana. *Dynamics of Multibody Systems*. Cambridge University Press, 2005.
- [45] Juhwan Choi, Han Sik Ryu, Chang Wan Kim, and Jin Hwan Choi. An efficient and robust contact algorithm for a compliant contact force model between bodies of complex geometry. *Multibody System Dynamics*, 23(1):99–120, 2010.
- [46] R C Hibbeler. *Engineering Mechanics Dynamics*. Pearson Prentice Hall, New Jersey, 12 edition, 2010.

- [47] G Gilardi and I Sharf. Literature survey of contact dynamics modelling. *Mechanism and Machine Theory*, 37(10):1213–1239, 2002.
- [48] W. Goldsmith. *Impact: The Theory and Physical Behaviour of Colliding Solids*. Edward Arnold, 1960.
- [49] WJ Stronge. *Impact Mechanics*. Cambridge university press, 1 edition, 2004.
- [50] Xiang Zhang and Loc Vu-Quoc. Modeling the dependence of the coefficient of restitution on the impact velocity in elasto-plastic collisions. *International Journal of Impact Engineering*, 27(3):317–341, 2002.
- [51] Paulo Flores and Jorge Ambrósio. On the contact detection for contact-impact analysis in multibody systems. *Multibody System Dynamics*, 24(1):103–122, 2010.
- [52] Xupeng Wang, Geng Liu, and Shangjun Ma. Dynamic analysis of planar mechanical systems with clearance joints using a new nonlinear contact force model. *Journal of Mechanical Science and Technology*, 30(4):1537–1545, 2016.
- [53] Bo Zhao, Kun Zhou, and You Bai Xie. A new numerical method for planar multibody system with mixed lubricated revolute joint. *International Journal of Mechanical Sciences*, 113:105–119, 2016.
- [54] Congcong Fang, Xianghui Meng, Xiaoli Kong, Bo Zhao, and Huang Huang. Transient tribo-dynamics analysis and friction loss evaluation of piston during cold- and warm-start of a SI engine. *International Journal of Mechanical Sciences*, 133:767–787, 2017.
- [55] Jorge Ambrosio and João Pombo. A unified formulation for mechanical joints with and without clearances/bushings and/or stops in the framework of multibody systems. *Multibody System Dynamics*, 42(3):317–345, 2018.
- [56] Narendra Akhadkar, Vincent Acary, and Bernard Brogliato. Multibody systems with 3D revolute joints with clearances: an industrial case study with an experimental validation. *Multibody System Dynamics*, pages 1–34, 2017.
- [57] Marcin Kapitaniak, Vahid Vaziri, Joseph Paéz Chávez, and Marian Wiercigroch. Numerical Study of Forward and Backward Whirling of Drill-String. *Journal of Computational and Nonlinear Dynamics*, 12(6):1–7, 2017.
- [58] Antonio S.E. Chong, Yuan Yue, Ekaterina Pavlovskaja, and Marian Wiercigroch. Global dynamics of a harmonically excited oscillator with a play: Numerical studies. *International Journal of Non-Linear Mechanics*, 94:98–108, 2017.
- [59] Dengqing Cao, Yang Yang, Huatao Chen, Deyou Wang, Guangyi Jiang, Chenggang Li, Jin Wei, and Kun Zhao. A novel contact force model for the impact analysis of structures with coating and its experimental verification. *Mechanical Systems and Signal Processing*, 70-71:1056–1072, 2016.
- [60] Morteza Azad and Roy Featherstone. (b) A New Nonlinear Model of Contact Normal Force (a) (b). 30(3):736–739, 2014.
- [61] Aline S De Paula, Marcelo A Savi, Vahid Vaziri, Ekaterina Pavlovskaja, and Marian Wiercigroch. Experimental bifurcation control of a parametric pendulum. *Journal of Vibration and Control*, 23(14):2256–2268, 2017.
- [62] Yang Liu, Haibo Jiang, Ekaterina Pavlovskaja, and Marian Wiercigroch. Experimental Investigation of the Vibro-impact Capsule System. *Procedia IUTAM*, 22:237–243, 2017.
- [63] Maolin Liao, James Ing, Mukthar Sayah, and Marian Wiercigroch. Dynamic method of stiffness identification in impacting systems for percussive drilling applications. *Mechanical Systems and Signal Processing*, 80:224–244, 2016.
- [64] Marcin Kapitaniak, Vahid Vaziri, Joseph Páez Chávez, and Marian Wiercigroch. Experimental studies of forward and backward whirls of drill-string. *Mechanical Systems and Signal Processing*, 100:454–465, 2018.
- [65] Margarida Machado, Pedro Moreira, Paulo Flores, and Hamid M. Lankarani. Compliant contact force models in multibody dynamics: Evolution of the Hertz contact theory. *Mechanism and Machine Theory*, 53(0):99–121, 2012.

- [66] Friedrich Pfeiffer. Energy considerations for frictional impacts. *Archive of Applied Mechanics*, 80(1):47–56, 2009.
- [67] Janete Alves, Nuno Peixinho, Miguel T. Da Silva, Paulo Flores, and Hamid M. Lankarani. A comparative study of the viscoelastic constitutive models for frictionless contact interfaces in solids. *Mechanism and Machine Theory*, 85:172–188, 2015.
- [68] Andre Roy and Juan A. Carretero. A damping term based on material properties for the volume-based contact dynamics model. *International Journal of Non-Linear Mechanics*, 47(3):103–112, 2012.
- [69] W. J. Stronge. Comment: collision with friction; part B: Poisson’s and Stronge’s hypotheses. *Multibody System Dynamics*, 24(1):123–127, 2010.
- [70] W. J. Stronge. Smooth dynamics of oblique impact with friction. *International Journal of Impact Engineering*, 51:36–49, 2013.
- [71] H. M. Lankarani and P. E. Nikravesh. A Contact Force Model With Hysteresis Damping for Impact Analysis of Multibody Systems. *Journal of Mechanical Design*, 112(3):369–376, 1990.
- [72] Janko Slavič and Miha Boltežar. Simulating multibody dynamics with rough contact surfaces and run-in wear. *Nonlinear Dynamics*, 45(3-4):353–365, 2006.
- [73] Valentina Beatini, Gianni Royer-Carfagni, and Alessandro Tasora. A regularized non-smooth contact dynamics approach for architectural masonry structures. *Computers & Structures*, 187:88–100, 2017.
- [74] Maria Fedorova and M. V. Sivaselvan. An algorithm for dynamic vehicle-track-structure interaction analysis for high-speed trains. *Engineering Structures*, 148:857–877, 2017.
- [75] Dan Negrut, Radu Serban, and Alessandro Tasora. Posing Multibody Dynamics with Friction and Contact as a Differential Complementarity Problem. *Journal of Computational and Nonlinear Dynamics*, (c), 2017.
- [76] Junhong Yue, Gui-Rong Liu, Ming Li, and Ruiping Niu. A cell-based smoothed finite element method for multi-body contact analysis using linear complementarity formulation. *International Journal of Solids and Structures*, 2018.
- [77] Cândida M. Pereira, Amílcar L. Ramalho, and Jorge A. Ambrósio. A critical overview of internal and external cylinder contact force models. *Nonlinear Dynamics*, 63(4):681–697, 2011.
- [78] Zheng Feng Bai and Yang Zhao. A hybrid contact force model of revolute joint with clearance for planar mechanical systems. *International Journal of Non-Linear Mechanics*, 48(1):15–36, 2013.
- [79] Qiang Tian, Paulo Flores, and Hamid M Lankarani. A comprehensive survey of the analytical , numerical and experimental methodologies for dynamics of multibody mechanical systems with clearance or imperfect joints. *Mechanism and Machine Theory*, 122:1–57, 2018.
- [80] Yulin Jin, Zhenyong Lu, Rui Yang, Lei Hou, and Yushu Chen. A new nonlinear force model to replace the Hertzian contact model in a rigid-rotor ball bearing system. *Applied Mathematics and Mechanics*, 39(3):365–378, 3 2018.
- [81] Heinrich Hertz. Ueber die Beruehrung fester elastischer Koerper. *Journal fuer die reine und angewandte Mathematik*, 91:156–171, 1881.
- [82] C. Pereira, A. Ramalho, and J. Ambrosio. Applicability domain of internal cylindrical contact force models. *Mechanism and Machine Theory*, 78:141–157, 2014.
- [83] Hamid M. Lankarani and Parviz E. Nikravesh. Continuous Contact Force Models for Impact Analysis in Multibody Systems. *Nonlinear Dynamics*, 5(2):193–207, 1994.
- [84] Luka Skrinjar, Janko Slavič, and Miha Boltežar. A validated model for a pin-slot clearance joint. *Nonlinear Dynamics*, 88(1):131–143, 2017.
- [85] Luka Skrinjar, Janko Slavič, and Miha Boltežar. Absolute Nodal Coordinate Formulation in a Pre-Stressed Large-Displacements Dynamical System. *Strojniški vestnik - Journal of Mechanical Engineering*, 63(7-8):417, 2017.

- [86] C Pereira, A Ramalho, and Jorge Ambrosio. An enhanced cylindrical contact force model. *Multibody System Dynamics*, 35(3):277–298, 2015.
- [87] C. Pereira, J. Ambrósio, and A. Ramalho. Dynamics of chain drives using a generalized revolute clearance joint formulation. *Mechanism and Machine Theory*, 92:64–85, 2015.
- [88] K. L. Johnson. *Contact Mechanics*. Cambridge University Press, London, 1995.
- [89] K. L. Johnson. One Hundred Years of Hertz Contact. *Pet Rev*, V 36(N 428):34–37, 1982.
- [90] Gholamhossein Lari. Identification of Compliant Contact Force Parameters in Multibody Systems Based on the Neural Network Approach Related to Municipal Property Damages. *American Journal of Neural Networks and Applications*, 3(5):49, 2017.
- [91] Thong M Pham, Yifei Hao, and Hong Hao. Sensitivity of impact behaviour of RC beams to contact stiffness. *International Journal of Impact Engineering*, 112:155–164, 2018.
- [92] Hossein Barikloo and Ebrahim Ahmadi. Dynamic Properties of Golden Delicious and Red Delicious Apple under Normal Contact Force Models. *Journal of Texture Studies*, 44(6):409–417, 2013.
- [93] P. E. Nikravesh. *Computer-Aided Analysis of Mechanical Systems*. Prentice-Hall, 1988.
- [94] S. Dubowsky and F. Freudenstein. Dynamic Analysis of Mechanical Systems With Clearances-Part 2: Dynamic Response. *Journal of Engineering for Industry*, 93(1):310–316, 2 1971.
- [95] S. Dubowsky and T. N. Gardner. Design and Analysis of Multilink Flexible Mechanisms With Multiple Clearance Connections. *J Eng Ind Trans ASME*, 99 Ser B(1):88–96, 1977.
- [96] T. Kakizaki, J. F. Deck, and S. Dubowsky. Modeling the Spatial Dynamics of Robotic Manipulators with Flexible Links and Joint Clearances. *Journal of Mechanical Design*, 115(4):839, 1993.
- [97] Y. A. Khulief and A. A. Shabana. A continuous force model for the impact analysis of flexible multibody systems. *Mechanism and Machine Theory*, 22(3):213–224, 1987.
- [98] B. Fox, L. S. Jennings, and a. Y. Zomaya. Numerical Computation of Differential-Algebraic Equations for Non-Linear Dynamics of Multibody Systems Involving Contact Forces. *Journal of Mechanical Design*, 123(2):272, 2001.
- [99] B. Brogliato, A. ten Dam, L. Paoli, F. Génot, and M. Abadie. Numerical simulation of finite dimensional multibody nonsmooth mechanical systems. *Applied Mechanics Reviews*, 55(2):107, 2002.
- [100] J. Ambrosio. Train kinematics for the design of railway vehicle components. *Mechanism and Machine Theory*, 45(8):1035–1049, 2010.
- [101] K. H. Hunt and F. R. E. Crossley. Coefficient of restitution interpreted as damping in vibroimpact. *Journal of Applied Mechanics*, (7):440–445, 1975.
- [102] T. M. Guess, G. Thiagarajan, M. Kia, and M. Mishra. A subject specific multibody model of the knee with menisci. *Medical Engineering and Physics*, 32(5):505–515, 2010.
- [103] Y. Gonthier, J. McPhee, C. Lange, and J. C. Piedboeuf. A regularized contact model with asymmetric damping and dwell-time dependent friction. *Multibody System Dynamics*, 11(3):209–233, 2004.
- [104] R. G. Herbert and D. C. McWhannell. Shape and frequency composition of pulses from an impact pair. *Journal of Engineering for Industry*, (99):513–518, 1977.
- [105] D. C. H. Yang and Z. S. Sun. A rotary model for spur gear dynamics. *Journal of Mechanisms, Transmissions and Automation in Design*, (107):529–535, 1985.
- [106] N. Sarkar, R. E. Ellis, and T. N. Moore. Backlash detection in geared mechanisms: modelling, simulation and experiments. *Mechanical Systems and Signal Processing*, (11):391–408, 1997.
- [107] T. W. Lee and A. C. Wang. On the dynamics of intermittent-motion mechanisms, Part 1: dynamic model and response. *Journal of Mechanisms, Transmissions, and Automation in Design*, (105):534–540, 1983.

- [108] S. Shivaswamy. *Modeling contact forces and energy dissipation during impact in multibody mechanical systems*. PhD thesis, Wichita State University, Wichita, Kansas, 1997.
- [109] A. L. Schwab, J. P. Meijaard, and P. Meijers. A comparison of revolute joint clearance models in the dynamic analysis of rigid and elastic mechanical systems. *Mechanism and Machine Theory*, 37:895–913, 2002.
- [110] P. Flores, J. Ambrosio, J. C. P. Claro, and H. M. Lankarani. Dynamic behaviour of planar rigid multi-body systems including revolute joints with clearance. *Proceedings of the Institution of Mechanical Engineers, Part K: Journal of Multi-body Dynamics*, 221(2):161–174, 2007.
- [111] O. Muvengi, J. Kihui, and B. Ikuu. Dynamic analysis of planar multi-body systems with LuGre friction at differently located revolute clearance joints. *Multibody System Dynamics*, 28(4):369–393, 2012.
- [112] Z. F. Bai and Y. Zhao. A hybrid contact force model of revolute joint with clearance for planar mechanical systems. *International Journal of Non-Linear Mechanics*, 48:15–36, 2013.
- [113] Q. Zhiying and L. Qishao. Analysis of impact process based on restitution coefficient. *Journal of Dynamics and Control* 4, page 294–298, 2006.
- [114] P. Flores, M. MacHado, M. T. Silva, and J. M. Martins. On the continuous contact force models for soft materials in multibody dynamics. *Multibody System Dynamics*, 25(3):357–375, 2011.
- [115] S. Hu and X. Guo. A dissipative contact force model for impact analysis in multibody dynamics. *Multibody System Dynamics*, 35(2):131–151, 2015.
- [116] Stavros a Anagnostopoulos. Pounding of buildings in series during earthquakes. *Earthquake Engineering and Structural Dynamics*, 16(March 1987):443–456, 1988.
- [117] Y. Tsuji, T. Tanaka, and T. Ishida. Lagrangian numerical simulation of plug flow of cohesionless particles in a horizontal pipe. *Powder Technology*, 71(3):239–250, 1992.
- [118] Jysoo Lee and Hans J. Herrmann. Angle of Repose and Angle of Marginal Stability: Molecular Dynamics of Granular Particles. pages 1–14, 1992.
- [119] J. Schäfer, S. Dippel, and D. E. Wolf. Force Schemes in Simulations of Granular Materials. *Journal de Physique I*, 6(1):5–20, 1996.
- [120] Robert Jankowski. Non-linear viscoelastic modelling of earthquake-induced structural pounding. *Earthquake Engineering and Structural Dynamics*, 34(6):595–611, 2005.
- [121] M. H. Bordbar and T. Hyppänen. Modeling of binary collision between multisize viscoelastic spheres. *Journal of Numerical Analysis, Industrial and Applied Mathematics*, 2(3-4):115–128, 2007.
- [122] T Schwager. Coefficient of normal restitution of viscous particles and cooling rate of granular gases. *Physical Review E*, 57(1):650–654, 1997.
- [123] Hongjian Zhang, Bernard Brogliato, and Caishan Liu. Dynamics of planar rocking-blocks with Coulomb friction and unilateral constraints: comparisons between experimental and numerical data. *Multibody System Dynamics*, 32(1):1–25, 2014.
- [124] Mohamed Gharib and Yildirim Hurmuzlu. A New Contact Force Model for Low Coefficient of Restitution Impact. *Journal of Applied Mechanics*, 79(6):064506, 2012.
- [125] Nikolai V. Brilliantov, Frank Spahn, Jan Martin Hertzsch, and Thorsten Pöschel. The collision of particles in granular systems. *Physica A: Statistical Mechanics and its Applications*, 231(4):417–424, 1996.
- [126] R. L. Burden and J. D. Faires. *Numerical Analysis*. 9 edition, 2011.
- [127] Hamid M. Lankarani and P. E. Nikravesh. Canonical Impulse-Momentum Equations for Impact Analysis of Multibody Systems. *Journal of Mechanical Design*, 114(1):180, 1992.
- [128] S. Ahmed, H. M. Lankarani, and M. F. O. S. Pereira. Frictional Impact Analysis in Open-Loop Multibody Mechanical Systems. *Journal of Mechanical Design*, 121(1):119–127, 1999.

- [129] Hamid M. Lankarani. A Poisson-Based Formulation for Frictional Impact Analysis of Multibody Mechanical Systems With Open or Closed Kinematic Chains. *Journal of Mechanical Design*, 122(4):489–497, 2000.
- [130] Shuting Li. A mathematical model and numeric method for contact analysis of rolling bearings. *Mechanism and Machine Theory*, 119:61–73, 2018.
- [131] Luka Skrinjar, Ales Turel, and Janko Slavič. DyS - Dynamics Simulation Software. <https://github.com/ladisk/DyS>, 2017.
- [132] C. S. Liu, K. Zhang, and R. Yang. The FEM analysis and approximate model for cylindrical joints with clearances. *Mechanism and Machine Theory*, 42(2):183–197, 2007.
- [133] R. J. Roark, W. C. Young, and R. Plunkett. *Formulas for Stress and Strain*, volume 43. 1976.
- [134] E. I. Radzimovsky. *Stress Distribution and Strength Condition of Two Rolling Cylinders Pressed Together*, volume 408. University of Illinois, 1953.
- [135] S Dubowsky and F Freudenstein. Dynamic Analysis of Mechanical Systems With Clearances-Part 1: Formation of Dynamic Model. *Journal of Engineering for Industry*, 93(1):305–309, 2 1971.
- [136] P. Flores, J. Ambrósio, J. C. P. Claro, and H. M. Lankarani. Influence of the contact–impact force model on the dynamic response of multi-body systems. *Proceedings of the Institution of Mechanical Engineers, Part K: Journal of Multi-body Dynamics*, 220(1):21–34, 2006.
- [137] ESDU-78035. *Contact phenomena I: stresses, deflections and contact dimensions for normally-loaded unlubricated elastic components*. Engineering Sciences Data Unit, London, 1978.
- [138] Bo N. J. Persson. *Sliding Friction: Physical Principles and Applications*. 2000.